

## Switching the Magnetization in Quantum Antiferromagnets

Katrin Bolsmann,<sup>\*</sup> Asliddin Khudoyberdiev<sup>†</sup>, and Götz S. Uhrig<sup>‡</sup>

*Condensed Matter Theory, Technische Universität Dortmund, Otto-Hahn-Straße 4, Dortmund 44221, Germany*



(Received 27 March 2023; accepted 31 July 2023; published 5 September 2023)

The orientation of the order parameter of quantum magnets can be used to store information in a dense and efficient way. Switching this order parameter corresponds to writing data. To understand how this can be done, we study a precessional reorientation of the sublattice magnetization in an (an)isotropic quantum antiferromagnet induced by an applied magnetic field. For this intriguing nonequilibrium issue, we introduce a description including the leading quantum and thermal fluctuations, namely time-dependent Schwinger boson mean-field theory, because this theory allows us to describe both ordered phases and the phases in between them, as is crucial for switching. An activation energy has to be overcome, requiring a minimum applied field  $h_c$  that is given essentially by the spin gap. It can be reduced significantly for temperatures approaching the Néel temperature, facilitating switching. The time required for switching diverges when the field approaches  $h_c$ , which is the signature of an inertia in the magnetization dynamics. The temporal evolution of the magnetization and of the energy reveals signs of dephasing. The switched state has lost a part of its coherence because the magnetic modes do not evolve in phase.

DOI: [10.1103/PRXQuantum.4.030332](https://doi.org/10.1103/PRXQuantum.4.030332)

### I. INTRODUCTION

Spintronics aims at exploiting the additional degree of freedom represented by the electron spin. In the early days of this very active field quantum antiferromagnets did not play a big role, seemingly corroborating Néel's famous quote "They are extremely interesting from the theoretical viewpoint, but do not seem to have any applications." [1]. Indeed, ferromagnets have an advantage in their ease of measurement and manipulation [2].

Contrary, however, to Néel's view, the focus of spintronic research in experiment and theory shifted towards antiferromagnets in the last years, as they have many advantages over ferromagnets [3]. Ferromagnetic domains, for instance, exhibit stray fields, which affect neighboring domains. This is detrimental for data storage and switching because adjacent bits influence one another. Since the stray-field interactions become the stronger the closer the bits are packed, the maximum density of bits is limited. But the era of big data and digitalization requires more

and more storage capacity in smaller and smaller physical space [4,5]. Loth *et al.* [6] demonstrated in 2012 that it is possible to substantially reduce the distance between antiferromagnetic bits compared to ferromagnetic bits due to the absence of stray fields.

Another significant advantage of antiferromagnets is that their eigenfrequencies are in the terahertz range while the ferromagnetic ones lie in the gigahertz range [7,8]. Thus one may expect that the typical times for manipulations are also shorter by a factor 1000 than in ferromagnets. These and other advantageous properties are the reason why measurement and control of antiferromagnets have become one of the most important fields of research in spintronics over the past decade [9].

There are various methods to read out the direction of the Néel vector of an antiferromagnet, even though it has no macroscopic magnetization. One way is by electrical measurements of the magnetoresistance [10,11], but there are also approaches based on optical means [12]. The manipulation of antiferromagnetic order has also been realized by various techniques [13–15]. In 2016, for instance, based on the theoretical predictions of Železný *et al.* [16], Wadley *et al.* [17] succeeded in switching the Néel vector of the antiferromagnet CuMnAs using current-induced internal fields.

In this work, we present a microscopic description of a two-dimensional anisotropic quantum antiferromagnet in and out of equilibrium based on spin-wave theory that captures the leading quantum and thermal fluctuations. Comparing the results with the numbers provided by more

<sup>\*</sup>katrin.bolsmann@tu-dortmund.de Present address: RWTH Aachen

<sup>†</sup>asliddin.khudoyberdiev@tu-dortmund.de

<sup>‡</sup>goetz.uhrig@tu-dortmund.de

*Published by the American Physical Society under the terms of the Creative Commons Attribution 4.0 International license. Further distribution of this work must maintain attribution to the author(s) and the published article's title, journal citation, and DOI.*

elaborate methods we estimate that they are correct within 30%. Thus, they provide a means to corroborate qualitative expectations by quantitative calculations although they are not yet highly precise.

Our main goal is to describe precessional switching of the sublattice magnetization by external magnetic fields. In our approach not only the magnetization at the zero and at the staggering wave vector is tracked, but *all* magnonic modes at *all* wave vectors. This includes the effects of dephasing, i.e., the fact that the modes evolve with different frequencies. This allows us to describe interference effects faithfully. Moreover, a description based on the elementary magnons also allows us to capture the influence of finite temperature, at least on the mean-field level. We emphasize that, to our knowledge, so far the theoretical approaches were based on the two vectors of the average magnetizations on the two sublattices; see the references above. Thus, our work reports conceptual and methodological progress apt to improve our understanding of the switching dynamics in quantum antiferromagnets.

Of course, spin-wave theory is a standard tool [18]. But the most common representations proposed by Holstein and Primakoff [19] or by Dyson and Maleev [20,21] start from a particular ordered state. The magnons describe only small deviations from one of the Néel states. In view of the goal to capture switching the magnetization from up-down on the two sublattices to down-up or vice versa, this is insufficient because the switching process includes the two antagonal Néel states. Starting from one of them and reaching its antipole implies far more than a small deviation. Hence, a suitable bosonic representation is required for which we use Schwinger bosons [18,22–25].

This representation does not use long-range order in a Néel state as the reference state, so it can describe even the disordered state. This also holds in ferromagnets [18,23,26,27]. Thus, even on the mean-field level, Schwinger bosons can capture large deviations from one of the ground states. We are aware that Schwinger boson mean-field theory may display pathologies in the form of spurious first-order transitions. But these are not likely in unfrustrated low-dimensional systems [28]. We use Schwinger bosons to describe the isotropic and anisotropic systems at equilibrium initially. Then, we demonstrate how this representation can be used to simulate the switching of the sublattice magnetization by means of an external magnetic field. We analyze how the system changes after the rotation and how the anisotropy and finite-temperature influence the switching. Thereby our study provides a basis for further theoretical investigations regarding the full control of quantum antiferromagnets, which in turn is expected to guide further experimental investigations.

The article is set up as follows. Section II introduces the model and its bosonic representation by Schwinger bosons. Then, Sec. III briefly recalls the corresponding mean-field theory in equilibrium for the isotropic and the anisotropic

Heisenberg antiferromagnets. Subsequently, we derive the equations of motion describing the dynamics in applied magnetic fields that induce precessional motion in Sec. IV. Finally, we summarize our results in Sec. V.

## II. HEISENBERG MODEL AND ITS SCHWINGER BOSON REPRESENTATION

### A. Heisenberg model and its Hamilton operator

We consider here the (an)isotropic Heisenberg model on a square lattice for a quantum antiferromagnet with localized spins  $S = 1/2$ . Its Hamilton operator reads

$$\mathcal{H} = \sum_{\langle i,j \rangle} \{J_{xy}(S_i^x S_j^x + S_i^y S_j^y) + J_z S_i^z S_j^z\}, \quad (1)$$

where  $i$  and  $j$  label sites of the underlying lattice, the sum runs over pairs of nearest neighbors counting each pair only once. Operators  $S_i^\alpha$  are the usual operators of the spin component  $\alpha$  at site  $i$ ; couplings  $J_z$  and  $J_{xy}$  are both antiferromagnetic, i.e., positive. We focus here on  $S = 1/2$  because this case implies the largest quantum fluctuations. In order to have an ordered phase at finite temperature, we consider the easy-axis model, taking  $J_z = J$  as the energy unit and defining the ratio  $\chi = J_{xy}/J_z \in [0, 1]$  so that the Hamiltonian can be rewritten as

$$\begin{aligned} \mathcal{H} &= J \sum_{\langle i,j \rangle} \chi (S_i^x S_j^x + S_i^y S_j^y) + S_i^z S_j^z \\ &= J \sum_{\langle i,j \rangle} \left\{ \frac{\chi}{2} (S_i^+ S_j^- + S_i^- S_j^+) + S_i^z S_j^z \right\}, \end{aligned} \quad (2)$$

where the spin ladder operators are used in the last step. We stress that the approach advocated below allows us to deal with larger spins and any form of spin anisotropy, for instance single-ion anisotropy as well.

For finite anisotropy  $\chi < 1$ , the magnons display a finite energy gap  $\Delta(\chi) > 0$ . In turn, the spin-spin correlation length  $\xi$  becomes finite following the estimate

$$\xi(\chi) = \frac{v}{\Delta(\chi)}, \quad (3)$$

where  $v$  is the spin-wave velocity. Below, we perform a calculation for finite clusters with linear dimension  $L$ . These will reflect the thermodynamic, infinite-size results whenever  $L \gg \xi$  holds.

A uniform magnetic field can be included by adding the term

$$\mathcal{H}_{\text{uni}} = -\mathbf{h} \cdot \sum_i \mathbf{S}_i, \quad (4)$$

while an alternating (staggered) magnetic field is accounted for by adding

$$\mathcal{H}_{\text{alt}} = -\mathbf{h}_{\text{alt}} \cdot \sum_i (-1)^i \mathbf{S}_i. \quad (5)$$

The length of vector  $\mathbf{h}$  is given as usual by  $g\mu_B B$ . In this article, the alternating field is applied along the  $z$  axis and the uniform field along the  $y$  axis.

### B. Schwinger boson representation

Introduced by Schwinger in 1952 [22], this representation uses two boson flavors  $a_i^{(\dagger)}$  and  $b_i^{(\dagger)}$  at site  $i$  to transform the spin operators as

$$S_i^+ = a_i^\dagger b_i, \quad (6a)$$

$$S_i^- = b_i^\dagger a_i, \quad (6b)$$

$$S_i^z = \frac{1}{2}(a_i^\dagger a_i - b_i^\dagger b_i), \quad (6c)$$

so that the spin commutation relations are reproduced. In contrast to the Holstein-Primakoff [19] and Dyson-Maleev bosons [20,21], both flavors of Schwinger bosons act on any lattice site and are not restricted to one sublattice. The physical meaning of the bosons can be explained best by taking a closer look at the expectation value

$$\langle S_i^z \rangle = \frac{1}{2}(\langle a_i^\dagger a_i \rangle - \langle b_i^\dagger b_i \rangle). \quad (7)$$

This corresponds to the difference between the mean occupation of the  $a$  bosons and  $b$  bosons at lattice site  $i$ . The expectation value  $\langle S_i^z \rangle$  is maximized if there are only  $a$  bosons at that lattice site and it is minimized if there are only  $b$  bosons. Expectation values lying between these two extremes are obtained by a mixture or a superposition of the two boson flavors. Given the finite value of the spin length  $S$ , it is obvious that the number of bosons per lattice site cannot be arbitrary since the expectation value of a spin along one axis can never be larger than  $S$ :  $|\langle S_i^z \rangle| \leq S$ . To guarantee that only the physical subspace is considered,  $\mathbf{S}_i^2 = S(S+1)$  must hold. This condition is equivalent to a local constraint on the number of bosons per lattice site, namely,

$$a_i^\dagger a_i + b_i^\dagger b_i = 2S \quad \text{for all } i \in \mathbb{N} \leq N. \quad (8)$$

In the mean-field approach, we refrain from fulfilling this constraint at each site. Instead, we include the constraint in the Hamiltonian as a Lagrange multiplier to ensure Eq. (8) on average. By creating a boson of one flavor and annihilating a boson of the other flavor, the ladder operators  $S^\pm$  in Eqs. (6a) and (6b) realize transitions between the eigenstates of different magnetic quantum numbers.

Using the Schwinger representation (6), the anisotropic antiferromagnetic Hamiltonian (2) reads

$$\begin{aligned} \mathcal{H} &= J \sum_{\langle i,j \rangle} \left\{ \frac{\chi}{2} (a_i^\dagger b_i b_j^\dagger a_j + a_j^\dagger b_j b_i^\dagger a_i) \right. \\ &\quad \left. + \frac{1}{4} (a_i^\dagger a_i - b_i^\dagger b_i) (a_j^\dagger a_j - b_j^\dagger b_j) \right\} \\ &= J \sum_{\langle i,j \rangle} \left\{ \frac{\chi}{2} (a_i^\dagger b_i b_j^\dagger a_j + a_j^\dagger b_j b_i^\dagger a_i) \right. \\ &\quad \left. + \frac{1}{4} (a_i^\dagger a_i a_j^\dagger a_j - a_i^\dagger a_i b_j^\dagger b_j - b_i^\dagger b_i a_j^\dagger a_j + b_i^\dagger b_i b_j^\dagger b_j) \right\}. \end{aligned} \quad (9)$$

The model can be extended to  $M$  flavors of the Schwinger bosons allowing for an  $SU(M)$  symmetry [18,29,30]. In this work, however, we stick to two boson flavors  $a$  and  $b$  since we deal with spin Hamiltonians with  $SU(2)$  symmetry.

## III. MEAN-FIELD THEORY OF THE EQUILIBRIUM

Here we briefly review the equilibrium solutions for the isotropic and the anisotropic cases for two reasons: (i) to introduce the notation and (ii) to provide the initial conditions for the magnetization switching considered in the following section. Some noticeable subtleties of the Schwinger boson description are given in the appendices.

### A. Spin isotropic case

By setting  $\chi = 1$ , the isotropic Schwinger Hamiltonian is obtained from Eq. (9):

$$\begin{aligned} \mathcal{H} &= \sum_{\langle i,j \rangle} \left\{ \frac{1}{2} (a_i^\dagger b_i b_j^\dagger a_j + a_j^\dagger b_j b_i^\dagger a_i) \right. \\ &\quad \left. + \frac{1}{4} (a_i^\dagger a_i a_j^\dagger a_j - a_i^\dagger a_i b_j^\dagger b_j - b_i^\dagger b_i a_j^\dagger a_j + b_i^\dagger b_i b_j^\dagger b_j) \right\}. \end{aligned} \quad (10)$$

We use the coupling constant  $J$  as the energy unit so that we can set it to unity. Defining the antiferromagnetic bond operator  $A_{ij} := a_i b_j - b_i a_j$ , the Hamiltonian can be rewritten as

$$\mathcal{H} = -\frac{1}{2} \sum_{\langle i,j \rangle} (A_{ij}^\dagger A_{ij} - 2S^2), \quad (11)$$

where constraint (8) was used. It is useful to rotate one sublattice by  $180^\circ$  about the  $y$  axis to obtain a uniform description of all lattice sites with full translational invariance. Note that this trick makes the Hamiltonian *and* the

antiferromagnetic phases translational invariant, facilitating their theoretical treatment. The precessional rotation studies below will be induced by an external magnetic field along the  $y$  axis that does not destroy the translation symmetry either. When rotating around the  $S^y$  axis, the  $x$  and  $z$  components of the spin operators change their signs. Consequently, in terms of Schwinger bosons, the substitution

$$a_j \rightarrow -b_j, \quad b_j \rightarrow a_j \quad (12)$$

is applied to one sublattice. The bond operator now reads

$$A_{ij} = a_i a_j + b_i b_j, \quad (13)$$

while the representation of Hamiltonian (11) remains unaltered. Defining the expectation value

$$A := \langle A_{ij} \rangle = \langle A_{ij}^\dagger \rangle \quad (14)$$

and replacing the quadrilinear terms by the terms with one or two contractions according to Wick's theorem, Hamiltonian (11) is converted to the mean-field Hamiltonian

$$\begin{aligned} \mathcal{H} = E_{\text{MF}} + \lambda \sum_i (a_i^\dagger a_i + b_i^\dagger b_i) \\ - \frac{1}{2} A \sum_{(i,j)} (a_i a_j + b_i b_j + \text{H.c.}) \end{aligned} \quad (15)$$

with the mean-field energy  $E_{\text{MF}} := N(A^2 + 2S^2)$ . Furthermore, to ensure that constraint (8) is always fulfilled on average, an additional sum with the Lagrange multiplier  $\lambda$  is added. The self-consistent diagonalization of this mean-field Hamiltonian is recalled in Appendix A in some detail for the sake of completeness.

### B. Spin anisotropic case

This case is more involved since the equations are less symmetric, which requires accounting for additional mean fields; see, for instance, Ref. [31]. Conceptually, however, there is an explicit difference in the anisotropic case between the two bosons so that no infinitesimal fields are needed to capture the long-range order.

By using constraint (8), the anisotropic Hamiltonian of the antiferromagnetic spin lattice (9) can be written as

$$\mathcal{H} = -\frac{1}{4} \sum_{(i,j)} \{(1 + \chi) A_{ij}^\dagger A_{ij} + (1 - \chi) B_{ij}^\dagger B_{ij} - 4S^2\} \quad (16)$$

with bond operators  $A_{ij} := a_i a_j + b_i b_j$  and  $B_{ij} := a_i a_j - b_i b_j$ . As before, one sublattice has been rotated by  $180^\circ$  using substitution (12) so that all spins point in the same

direction in the ordered phase, achieving a fully translational invariant description. The mean-field Hamiltonian is obtained by applying Wick's theorem, neglecting quadrilinear normal-ordered terms:

$$\begin{aligned} \mathcal{H} = E_{\text{MF}} + \lambda \sum_i (a_i^\dagger a_i + b_i^\dagger b_i) \\ - \frac{1}{4} \sum_{(i,j)} \{A(1 + \chi)(a_i a_j + b_i b_j + \text{H.c.}) \\ + B(1 - \chi)(a_i a_j - b_i b_j + \text{H.c.})\} \end{aligned} \quad (17)$$

with  $E_{\text{MF}} := \frac{1}{2} N \{A^2(1 + \chi) + B^2(1 - \chi) + 4S^2\}$  and the expectation values  $A := \langle A_{ij} \rangle = \langle A_{ij}^\dagger \rangle$  and  $B := \langle B_{ij} \rangle = \langle B_{ij}^\dagger \rangle$ . For later use, we introduce the combinations

$$C_\pm := (A(1 + \chi) \mp B(1 - \chi)). \quad (18)$$

Furthermore, a boson number term with the Lagrange multiplier  $\lambda$  is added to ensure that constraint (8) is also satisfied in the anisotropic case on average. With vanishing anisotropy  $\chi \rightarrow 1$ , this Hamiltonian corresponds to that of the isotropic system (15).

Figure 1 depicts the spin gap and compares it with recently published data obtained by a different advanced semianalytical approach using continuous similarity transformations (CSTs) [32]. The latter can be considered to be exact within line width. Good agreement is obtained if the CST data are rescaled by the factor 1.3. In view of the simplicity of the mean-field approach, this agreement is quite good. In particular, mean-field and CST results are consistent with a square root behavior,  $\Delta \propto (1 - \chi^2)^\mu$ , even though fitting indicates slightly larger exponents,  $\mu \approx 0.54$ . This finding supports evidence that the mean-field approximation provides quantitative results within 30%.

In order to determine the magnetization, we rewrite Eq. (7) in terms of the  $\alpha$  and  $\beta$  particles and explicitly obtain

$$m_0 = \frac{\lambda}{4N} \sum_{\mathbf{k}} \left[ \frac{\coth(\beta \omega_{\mathbf{k}}^- / 2)}{\omega_{\mathbf{k}}^-} - \frac{\coth(\beta \omega_{\mathbf{k}}^+ / 2)}{\omega_{\mathbf{k}}^+} \right]. \quad (19)$$

Its evaluation at  $T = 0$  is given in Appendix A 2, yielding

$$m_0 = S + \frac{1}{2} - \frac{1}{8\pi^2} \int_{\text{BZ}} dk^2 \frac{C_-}{\sqrt{C_-^2 - C_+^2 \gamma_{\mathbf{k}}^2}}. \quad (20)$$

The resulting data are also given in Appendix A 2.

### C. Finite temperature

Here we turn to the effect of finite temperature. We are not interested in the phase without order occurring at high temperatures above the Néel temperature  $T_N$ . In the ordered phase, a difference between the dispersion of

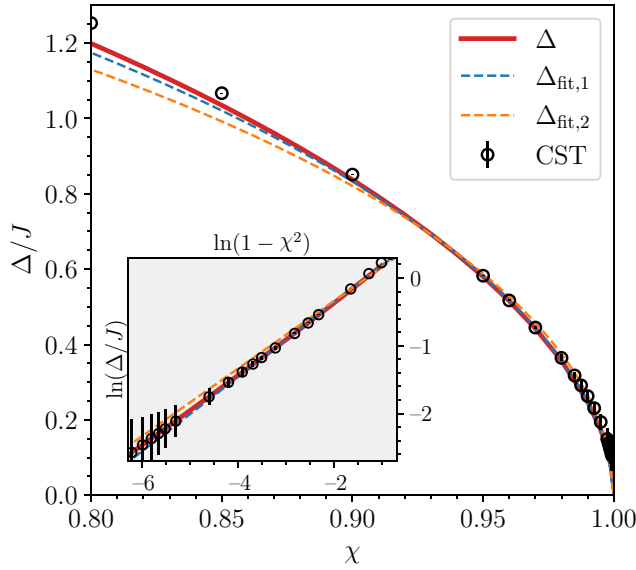


FIG. 1. The spin gap  $\Delta$  plotted as a function of the anisotropy  $\chi$ . The red solid curve shows the Schwinger boson mean-field data while the dashed curves are fits:  $\Delta_{\text{fit},i} = c_i(1 - \chi^2)_i^\mu$  with  $c_1 = (2.04 \pm 0.06)J$ ,  $\mu_1 = 0.54 \pm 0.02$  (blue curve) and with  $c_2 = (1.88 \pm 0.06)J$ ,  $\mu_2 = 1/2$  (orange curve). The black symbols represent gap values obtained by CST [32] rescaled by the factor 1.3.

the  $\alpha$  boson and the  $\beta$  boson persists. In contrast, however, to zero temperature no condensation of either boson occurs. Both bosons become gapped at finite temperature. Note that this does not imply that there is no longer a finite sublattice magnetization  $m_0$  because the anisotropy ensures that  $m_0 \neq 0$  is also possible up to some finite Néel temperature.

For simplicity and for later use, we consider a finite mesh of the Brillouin zone on which we evaluate the expectation values required to determine  $A$ ,  $B$ , and the Lagrange parameter  $\lambda$  self-consistently; see also Sec. IV. This is done for systems with linear extension up to  $L = 200$  at finite temperature and up to  $L = 500$  at zero temperature so that finite-size effects are very small and negligible. In order to find the self-consistent solution of the ordered phase in practical implementations, one must start from initial guesses for the parameters that allow for a difference between the  $\alpha$  and the  $\beta$  bosons. This means that one has to start with some finite  $B > 0$ .

Figure 19 in Appendix A 2 illustrates the resulting dispersions  $\omega_{\mathbf{k}}^-$  of the  $\alpha$  boson and  $\omega_{\mathbf{k}}^+$  of the  $\beta$  boson. As stated before, both are gapped. But, for positive  $m_0$ , the dispersion  $\omega_{\mathbf{k}}^-$  is still lower than the dispersion  $\omega_{\mathbf{k}}^+$  so that more  $a$  bosons are present than  $b$  bosons. We define the gaps

$$\Delta^\pm := \omega_{\mathbf{k}=0}^\pm, \quad (21a)$$

$$\Delta := \Delta^+ - \Delta^-. \quad (21b)$$

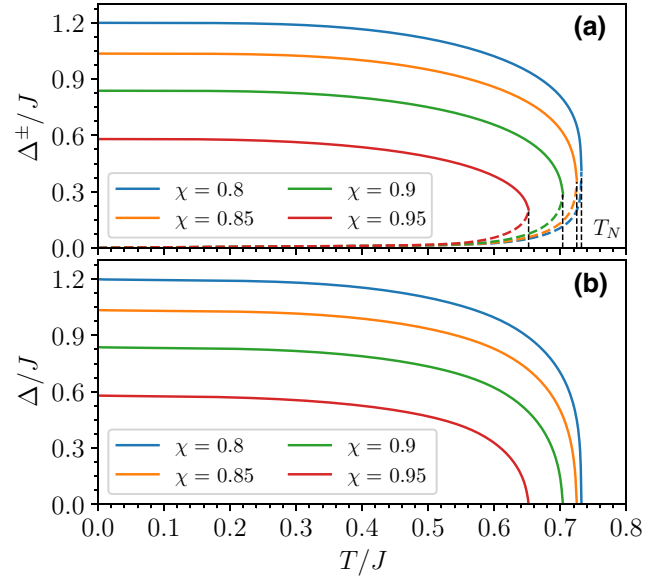


FIG. 2. (a) Auxiliary gaps  $\Delta^\pm$  as a function of temperature for various anisotropies  $\chi$ . Gap  $\Delta^+$  shown with solid lines refers to  $\beta$  bosons; gap  $\Delta^-$  shown with dashed lines refers to  $\alpha$  bosons. The two gaps merge at the Néel temperature  $T_N$  indicated by short vertical black lines. (b) Effective physical gap  $\Delta$  according to Eq. (21b).

The gaps  $\Delta^\pm$  are auxiliary quantities without direct physical meaning because the physical spin excitations always imply an action on two bosons. In particular, the annihilation of an  $\alpha$  boson and the creation of a  $\beta$  boson represents a spin flip down for  $S = 1/2$  or generally a lowering of the sublattice magnetization by the creation of one magnon. Thus, the above quantity  $\Delta$  represents the physical spin gap. Figure 2 displays the auxiliary gaps  $\Delta^\pm$  in panel (a) and the physical gap  $\Delta$  in panel (b). In a rigorous treatment, the spin gap is a property at  $T = 0$  referring to the minimum energy between the ground state and the first excited state(s). In this view, no “temperature-dependent” spin gap makes sense. The spin gap in a mean-field theory must be seen as an *effective* spin gap that reflects the gap of the bilinear mean-field Hamiltonian that describes the physics of the underlying interacting model best at a given temperature. In computations of the dynamical structure factor care must be taken to ensure that no leftovers of single Schwinger boson excitations remain. This issue has been resolved only very recently [33].

Once we know all the expectation values in reciprocal space we also know all expectation values in real space. Thus, the sublattice magnetization can also be computed and it is displayed as a function of temperature in Fig. 3 up to the respective Néel temperatures. The power law close to the Néel temperatures is expected to be a square root law as is generic for mean-field theories and our data are fully consistent with this assumption. The analogous square root

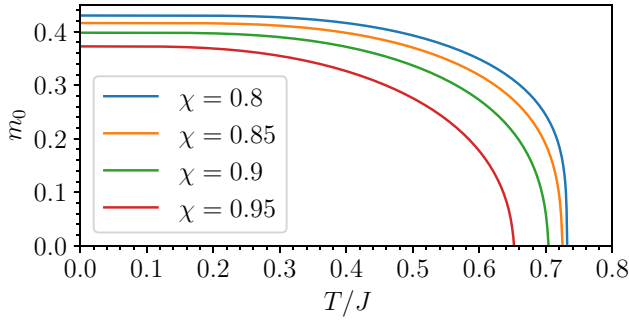


FIG. 3. Sublattice magnetization  $m_0$  as defined in Eq. (7) for various anisotropies  $\chi$  as a function of temperature. The solid line is a guide to the eye. It vanishes at the Néel temperature, where the ordered phase ceases to exist, with a square root behavior.

law is consistent with our findings for the effective spin gap  $\Delta$  in Fig. 2(b).

Finally, Fig. 4 depicts the Néel temperature as a function of the anisotropy according to the Schwinger boson mean-field theory. As pointed out before, this mean-field theory complies with the rigorous Mermin-Wagner theorem [34] so that  $\lim_{\chi \rightarrow 1} T_N(\chi) = 0$  holds. But the downturn upon approaching the isotropic case is extremely steep. From the integrals in the derivation of the Mermin-Wagner theorem for two dimensions, a logarithmic dependence according to  $T_N/J \approx c_1/(|\ln(1-\chi)| + c_2)$  appears plausible; see the caption. To estimate the accuracy of our results, we can compare them at  $\chi = 0$  with the rigorous result of Onsager [35] for the two-dimensional Ising model yielding  $T_N = 0.5673J$ . As for the gap, the results agree if the mean-field results are scaled down by a factor of 1.3. We emphasize that this result provides an estimate of the accuracy of the mean-field Schwinger approach even far away from the ground state. Hence, even for a significant occupation of both flavors, the mean-field treatment of their interaction leads to good results within 30% of the correct values. This also justifies the use of this approach for switching processes that take the system far away from their ground states as well.

The results presented in this section provide an overview of the essential properties of the system in equilibrium. It is crucial to know them quantitatively because they define the initial conditions for the subsequent time-dependent solutions that describe the switching process.

#### IV. SWITCHING THE SUBLATTICE MAGNETIZATION

The aim is to invert the sublattice magnetization  $m_0 \rightarrow -m_0$ . We denote the time-dependent sublattice magnetization during the switching process by  $m(t)$ . One can think of this process as switching a bit from its 1 state to its 0 state.

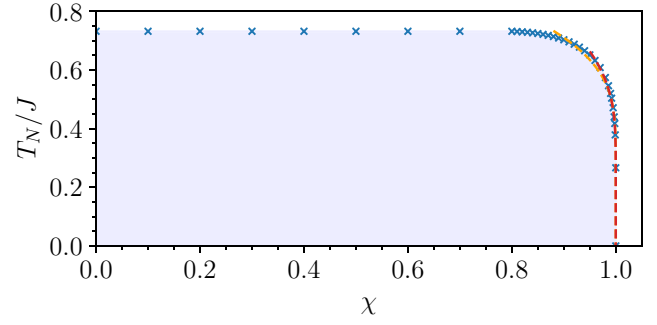


FIG. 4. Néel temperature as a function of the anisotropy. In accord with the Mermin-Wagner theorem, the Néel temperature vanishes in the isotropic case, i.e., for  $\chi \rightarrow 1$ . The vanishing of  $T_N$  close to the isotropic point can be fitted according to  $T_N/J \approx c_1/(|\ln(1-\chi)| + c_2)$  with  $c_1 = 4.1 \pm 0.08$  and  $c_2 = 3.5 \pm 0.02$  in the interval  $\chi \in [0.88, 1]$  (orange dashed line) and with  $c_1 = 3.5 \pm 0.05$  and  $c_2 = 2.3 \pm 0.06$  in the interval  $\chi \in [0.95, 1]$  (red dashed line).

Hence, the considered process is highly relevant in data storage with the advantages exposed in the Introduction.

We have a precessional rotation in mind. Thus we add a static magnetic field along the  $S^y$  axis in form of a Zeeman term from time  $t = 0$  onwards:

$$\begin{aligned} \mathcal{H} &= \mathcal{H}_0 - h_y \sum_i S_i^y \\ &= \mathcal{H}_0 - \frac{h_y}{2i} \sum_i (S_i^+ - S_i^-) \\ &= \mathcal{H}_0 - \frac{h_y}{2i} \sum_i (a_i^\dagger b_i - b_i^\dagger a_i) \end{aligned} \quad (22)$$

with  $\mathcal{H}_0$  the unperturbed Hamiltonian (15).

For the isotropic case, the Zeeman term does not change under the Bogoliubov transformation, yielding

$$\begin{aligned} \mathcal{H} &= E_{\text{MF}} - N\lambda + \sum_{\mathbf{k}} \omega_{\mathbf{k}}^{\text{iso}} (\alpha_{\mathbf{k}}^\dagger \alpha_{\mathbf{k}} + \beta_{\mathbf{k}}^\dagger \beta_{\mathbf{k}} + 1) \\ &\quad - \frac{h_y}{2i} \sum_{\mathbf{k}} (\alpha_{\mathbf{k}}^\dagger \beta_{\mathbf{k}} - \beta_{\mathbf{k}}^\dagger \alpha_{\mathbf{k}}). \end{aligned} \quad (23)$$

Because of the spin isotropy, the Zeeman term commutes with the Hamiltonian so that any ground state of  $\mathcal{H}_0$  remains a ground state under the action of the Zeeman term. The Zeeman term induces a collective rotation about  $S^y$  at all sites simultaneously. The rotation of each spin can be treated as if the spin were isolated. Hence, the sublattice magnetization is rotated in the  $S^z$ - $S^x$  plane. A rotation about the angle  $\varphi$  is achieved within the time interval

$$t_\varphi = \frac{\varphi}{h_y}. \quad (24)$$

This can be verified in terms of the spin operators or in terms of the Schwinger bosons. The tilt  $m_0 \rightarrow -m_0$  is achieved for  $t_\pi = \pi/h_y$ . No minimum magnetic field is required to achieve the rotation if one can create long enough pulses of constant magnetic fields. Yet, this case is not promising for application because the absence of any anisotropy also implies that the system does not have any rigidity of the sublattice magnetization against perturbations.

For this reason, we turn to the anisotropic case where the situation is more subtle because the Zeeman term does not commute with the Hamiltonian. We have to compute the time evolution under the full mean-field Hamiltonian

$$\begin{aligned} \mathcal{H} = E_{\text{MF}} - \frac{1}{2} \sum_{\mathbf{k}} \gamma_{\mathbf{k}} (C_- a_{\mathbf{k}}^\dagger a_{-\mathbf{k}}^\dagger + C_+ b_{\mathbf{k}}^\dagger b_{-\mathbf{k}}^\dagger \\ + C_-^* a_{\mathbf{k}} a_{-\mathbf{k}} + C_+^* b_{\mathbf{k}} b_{-\mathbf{k}}) \\ + \lambda \sum_{\mathbf{k}} (a_{\mathbf{k}}^\dagger a_{\mathbf{k}} + b_{\mathbf{k}}^\dagger b_{\mathbf{k}}) - \frac{h_y}{2i} \sum_{\mathbf{k}} (a_{\mathbf{k}}^\dagger b_{\mathbf{k}} - b_{\mathbf{k}}^\dagger a_{\mathbf{k}}). \end{aligned} \quad (25)$$

We stress that the prefactors  $C_\pm$  defined in Eq. (18) depend on expectation values that themselves acquire a temporal dependence upon switching. Hence, the above Hamiltonian itself is time dependent. We refrain from expressing Hamiltonian (25) in terms of Bogoliubov particles  $\alpha_{\mathbf{k}}$  and  $\beta_{\mathbf{k}}$  because no useful simplification can be reached due to the time dependence of the  $C_\pm$ . It would be required to adjust the Bogoliubov transformation at each instant of time in order to keep diagonality. The ensuing numerics would be unnecessarily tedious and would eventually yield the same results. So no additional insight or advantage would be reached.

Hamiltonian (25) is fully sufficient to compute the time dependence of the expectation values by means of Heisenberg's equations of motion. This amounts to the density-matrix formalism. The set of differential equations reads

$$\partial_t \langle a_{\mathbf{k}}^\dagger a_{\mathbf{k}} \rangle = 2\gamma_{\mathbf{k}} \Im(C_-^* \langle a_{\mathbf{k}} a_{-\mathbf{k}} \rangle) + \frac{h_y}{2} (\langle a_{\mathbf{k}}^\dagger b_{\mathbf{k}} \rangle + \langle b_{\mathbf{k}}^\dagger a_{\mathbf{k}} \rangle), \quad (26a)$$

$$\partial_t \langle b_{\mathbf{k}}^\dagger b_{\mathbf{k}} \rangle = 2\gamma_{\mathbf{k}} \Im(C_+^* \langle b_{\mathbf{k}} b_{-\mathbf{k}} \rangle) - \frac{h_y}{2} (\langle a_{\mathbf{k}}^\dagger b_{\mathbf{k}} \rangle + \langle b_{\mathbf{k}}^\dagger a_{\mathbf{k}} \rangle), \quad (26b)$$

$$\begin{aligned} \partial_t \langle a_{\mathbf{k}}^\dagger b_{\mathbf{k}} \rangle = -i\gamma_{\mathbf{k}} (C_-^* \langle a_{\mathbf{k}} b_{-\mathbf{k}} \rangle - C_+ \langle a_{\mathbf{k}}^\dagger b_{-\mathbf{k}}^\dagger \rangle) \\ + \frac{h_y}{2} (\langle b_{\mathbf{k}}^\dagger b_{\mathbf{k}} \rangle - \langle a_{\mathbf{k}}^\dagger a_{\mathbf{k}} \rangle), \end{aligned} \quad (26c)$$

$$\begin{aligned} \partial_t \langle a_{\mathbf{k}} a_{-\mathbf{k}} \rangle = i\gamma_{\mathbf{k}} [C_- (2\langle a_{\mathbf{k}}^\dagger a_{\mathbf{k}} \rangle + 1)] \\ - 2\lambda i \langle a_{\mathbf{k}} a_{-\mathbf{k}} \rangle + h_y \langle a_{\mathbf{k}} b_{-\mathbf{k}} \rangle, \end{aligned} \quad (26d)$$

$$\begin{aligned} \partial_t \langle b_{\mathbf{k}} b_{-\mathbf{k}} \rangle = i\gamma_{\mathbf{k}} [C_+ (2\langle b_{\mathbf{k}}^\dagger b_{\mathbf{k}} \rangle + 1)] \\ - 2\lambda i \langle b_{\mathbf{k}} b_{-\mathbf{k}} \rangle - h_y \langle a_{\mathbf{k}} b_{-\mathbf{k}} \rangle, \end{aligned} \quad (26e)$$

$$\begin{aligned} \partial_t \langle a_{\mathbf{k}} b_{-\mathbf{k}} \rangle = i\gamma_{\mathbf{k}} (C_- \langle a_{\mathbf{k}}^\dagger b_{\mathbf{k}} \rangle + C_+ \langle a_{\mathbf{k}}^\dagger b_{\mathbf{k}} \rangle^*) - 2\lambda i \langle a_{\mathbf{k}} b_{-\mathbf{k}} \rangle \\ - \frac{h_y}{2} (\langle a_{\mathbf{k}} a_{-\mathbf{k}} \rangle - \langle b_{\mathbf{k}} b_{-\mathbf{k}} \rangle). \end{aligned} \quad (26f)$$

These equations are ordinary first-order differential equations in time. Their main complexity results from the nonlinearity embodied in the dependence of coefficients  $C_\pm$  on the expectation values; see below. The equations are solved by the Runge-Kutta algorithm of fourth order as implemented in the Boost Odeint library.

In terms of the initial Schwinger bosons without any Bogoliubov transformations, the relations defining  $A$ ,  $B$ , and the constraint read

$$A = \langle a_i a_j \rangle + \langle b_i b_j \rangle = \frac{1}{N} \sum_{\mathbf{k}} \gamma_{\mathbf{k}} (\langle a_{\mathbf{k}} a_{-\mathbf{k}} \rangle + \langle b_{\mathbf{k}} b_{-\mathbf{k}} \rangle), \quad (27a)$$

$$B = \langle a_i a_j \rangle - \langle b_i b_j \rangle = \frac{1}{N} \sum_{\mathbf{k}} \gamma_{\mathbf{k}} (\langle a_{\mathbf{k}} a_{-\mathbf{k}} \rangle - \langle b_{\mathbf{k}} b_{-\mathbf{k}} \rangle), \quad (27b)$$

$$2S = \langle a_i^\dagger a_i \rangle + \langle b_i^\dagger b_i \rangle = \frac{1}{N} \sum_{\mathbf{k}} (\langle a_{\mathbf{k}}^\dagger a_{\mathbf{k}} \rangle + \langle b_{\mathbf{k}}^\dagger b_{\mathbf{k}} \rangle), \quad (27c)$$

where  $i, j$  are adjacent sites. This completes a closed set of differential equations. Constraint (27c) is not needed for the temporal equation. But we checked that it is always fulfilled in the course of time if it is fulfilled initially, as is ensured by starting from a valid equilibrium solution.

### A. Switching at zero temperature

Figure 5 displays the dynamics of the occupations of the Schwinger bosons and the resulting sublattice magnetization  $m(t)$  given by

$$m(t) = \frac{1}{2} (\langle a_i^\dagger a_i \rangle - \langle b_i^\dagger b_i \rangle) = \frac{1}{2N} \sum_{\mathbf{k}} (\langle a_{\mathbf{k}}^\dagger a_{\mathbf{k}} \rangle - \langle b_{\mathbf{k}}^\dagger b_{\mathbf{k}} \rangle) \quad (28)$$

for various values of the anisotropy parameter  $\chi$ . Panel (a) shows the result for the isotropic case. The external field applied perpendicular to the sublattice magnetization  $m_0$  nicely rotates it following a cosine curve to  $-m_0$  at time  $t_\pi$  predicted by Eq. (24). Since the switching field persists, the magnetization is switched back to the initial value at  $t = 2t_\pi$ . No reduction of  $m$  due to dephasing is discernible; the rotation is fully coherent.

Figure 5(b) reveals differences to the isotropic case. First, the initial magnetization is larger in agreement with the results shown in Fig. 18 in Appendix A 2. The

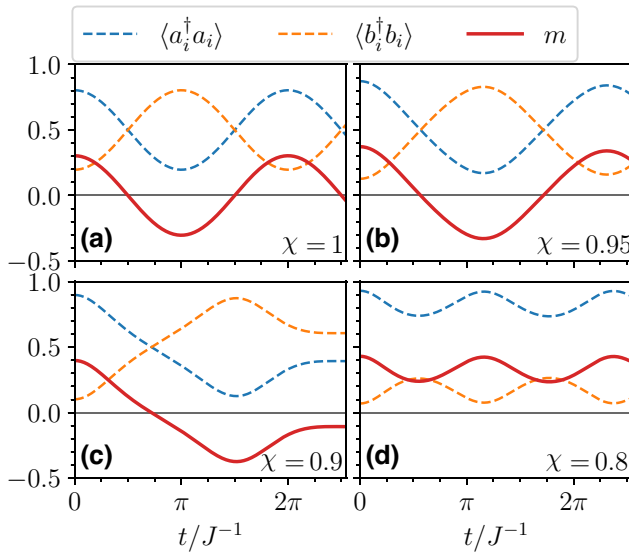


FIG. 5. Dynamics of the occupation of the Schwinger bosons  $\langle a_i^\dagger a_i \rangle$  and  $\langle b_i^\dagger b_i \rangle$ , as well as the resulting magnetization  $m$  in the time interval  $t \in [0J^{-1}, 8J^{-1}]$  for exemplary values of the anisotropy: panel (a) for  $\chi = 1$ , panel (b) for  $\chi = 0.95$ , panel (c) for  $\chi = 0.9$ , and panel (d) for  $\chi = 0.8$ . The strength of the applied field is  $h = 1J$  so that in the isotropic case [panel (a),  $\chi = 1$ ], the switching duration of  $t = \pi J^{-1}$  for the  $\pi$  pulse results in accord with Eq. (24). The calculations were performed for a system size of  $L = 500$ , implying that  $N = 250\,000$ .

switching to negative values of  $m$  succeeds, but it takes longer than in the isotropic case. We attribute this to the anisotropy that hinders the rotation taking place although the state with sublattice magnetization  $-m_0$  is also a valid ground state. But the states in between are neither ground states nor eigenstates of the system. This leads to dephasing of the modes at different wave vectors and implies that  $|m(t)|$  does not reach the initial value  $m_0$  anymore. This appears physically plausible and was to be expected on the basis of the symmetries of the model. But we emphasize that this behavior cannot be found in the so far mostly used classical two-vector model; to our knowledge, the time-dependent Schwinger approach advocated here is the first that captures this important physical feature.

Increasing the anisotropy by lowering  $\chi$  we see an even longer switching process in Fig. 5(c). Surprisingly, only one switching appears to be possible since the switching back to the original sign of  $m$  does not take place. We investigated the long-time behavior up to  $t = 100/J$  and the magnetization continued to fluctuate weakly in the vicinity  $m_0 \approx -0.4$ . Thus, the switched modes appear to be out of phase, i.e., dephasing has been quite detrimental. We reemphasize that such effects are not captured by the description of the sublattice magnetization by a classical vector. Finally, panel (d) displays an example where no switching occurs at all. The sublattice magnetization oscillates only a little below its initial value  $m_0$ .

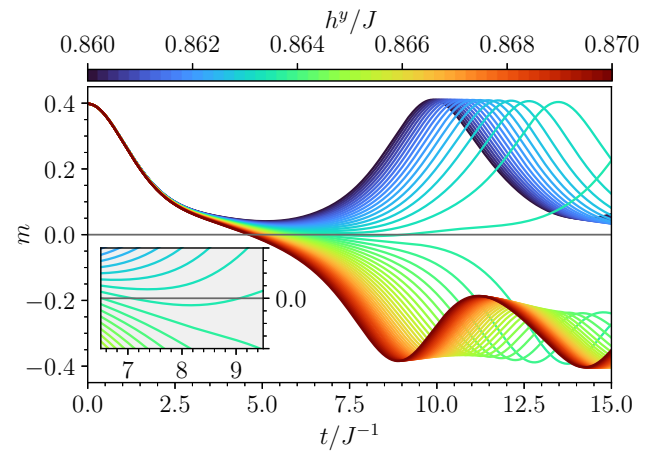


FIG. 6. Time evolution of the magnetization  $m$  for various external fields  $h^y \in [0.86J, 0.87J]$  at the anisotropy  $\chi = 0.9$ . The color bar on top indicates the external field. Clearly, qualitatively distinct temporal behaviors occur depending on the strength of the applied magnetic field. There is a threshold value  $h_t$  above which switching is possible and below which no switching is possible.

These observations show that a minimum magnetic field is required in order to change the sign of  $m$ . The anisotropy generates a degree of robustness that needs to be overcome by the external magnetic field.

In order to further investigate the conditions for successful switching, we scan  $m(t)$  for a range of applied magnetic fields in Fig. 6. We observe a distinct difference in the behavior for lower fields compared to the behavior for larger ones. Large ones enable switching and low ones do not. There is a well-defined value  $h_t$  separating the two regimes. We define a criterion to distinguish whether switching is possible or not. The occurrence of a negative value of  $m(t)$  is not the perfect high-precision criterion. The inset of Fig. 6 shows that it can occur that  $m(t)$  takes slightly negative values, but turns back to positive values. Instead, we choose the occurrence of an inflection point before the first extremal value at  $t > 0$  as a criterion. If such an inflection point exists,  $m(t)$  continues to turn down, reaching a substantial negative value. Otherwise, it appears that no switching is possible. But we stress that the difference between the criterion based on the inflection and that based on the sign change is minor.

Next, we quantify how long the switching takes. Duration  $t$  is the instant in time when the negative minimum is reached. If no switching is possible, we define the instant in time when the positive maximum is reached as the duration of the failed switching attempt. These durations are plotted in Fig. 7 together with suitable logarithmic fits

$$t_{\text{fit}}(h^y) = c_1 + c_2 \ln |(h^y - h_t)/J|. \quad (29)$$

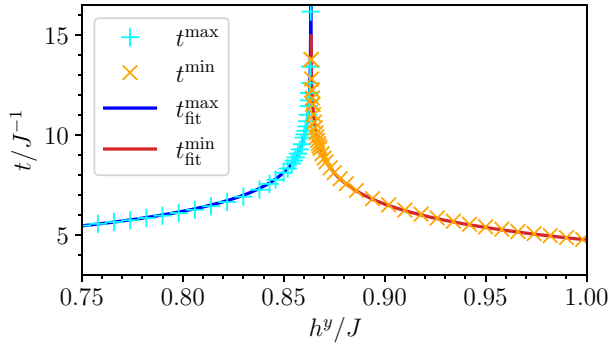


FIG. 7. Times (symbols) at which  $m(t)$  reaches the relevant minimum or maximum, depending on whether switching is possible (orange) or not (cyan) plotted against the external field  $h^y$  for  $\chi = 0.9$ . The position of the singularity defines the threshold field  $h_t$ . More data points were computed around the singularity to obtain a higher accuracy for fitting the function given in Eq. (29).

The fits describe the data remarkably well below and above the threshold with very similar parameters for the minima (succeeded switching)

$$c_1^{\min} = (2.04 \pm 0.06)J^{-1}, \quad (30a)$$

$$c_2^{\min} = (-1.36 \pm 0.01)J^{-1}, \quad (30b)$$

$$h_t^{\min} = (0.8634 \pm 5 \times 10^{-6})J, \quad (30c)$$

and for the maxima (failed switching)

$$c_1^{\max} = (2.73 \pm 0.08)J^{-1}, \quad (31a)$$

$$c_2^{\max} = (-1.25 \pm 0.01)J^{-1}, \quad (31b)$$

$$h_t^{\max} = (0.8634 \pm 6 \times 10^{-7})J. \quad (31c)$$

Clearly, the resulting threshold value for  $\chi = 0.9$  is  $(0.8634 \pm 5 \times 10^{-6})J$ , which is quite substantial and fairly close to the value of the spin gap  $\Delta$ . The question suggests itself why such a logarithmic divergence occurs. We argue that this kind of divergence is a clear signature that the magnetic order in antiferromagnets has a certain inertia in its dynamics. This was observed in experiment and supported by a calculation based on classical equations of motion for the antiferromagnetic vector describing the size and direction of the sublattice magnetization [13]. The fact that the microscopic spin-wave description reproduces this behavior corroborates the idea of an inertia of the antiferromagnetic order convincingly. In Appendix B we show that a classical motion of a massive particle over an activation barrier reproduces the logarithmic singularity that we observed. This supports the above interpretation.

We determine these threshold values of a range of anisotropies by bisection with high accuracy. The resulting data are shown in Fig. 8 by the symbols. We compare

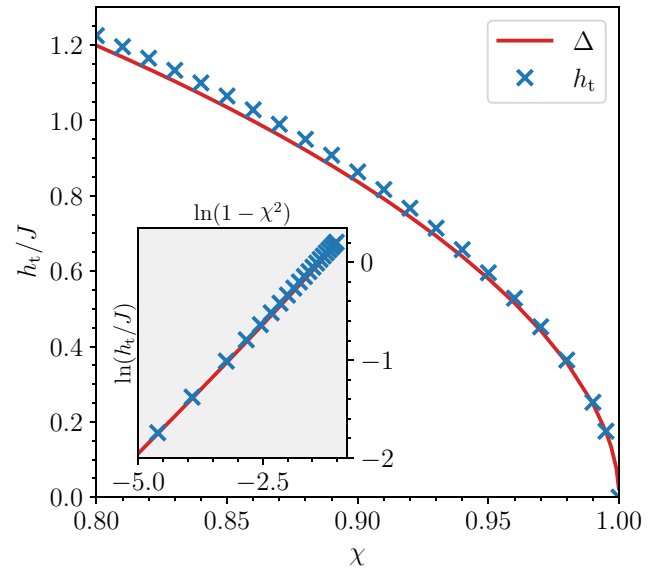


FIG. 8. Threshold magnetic field  $h_t$  depicted by the blue symbols versus anisotropy  $\chi$ . The data are obtained for a system size  $L = 500$ . The red solid curve reproduces the spin gap from Fig. 1 to illustrate that the threshold magnetic fields are essentially determined by the size of the spin gap.

them with the values of the spin gap shown above in Fig. 1. They are very close to each other for the shown range of anisotropies. Thus, we conclude that it is the size of the spin gap that determines the typical field strength required for switching. This is in line with the idea that the spin gap measures the robustness of the system against any kind of perturbation.

We emphasize that a key aspect of the description of the switching dynamics in terms of spin waves is that the contribution of each mode is captured individually. The whole process is not one single collective motion, but it consists of the contributions of a thermodynamically large number of modes. Hence, the coherence is not preserved in the course of the switching process except in the isotropic case. This could already be inferred from the decrease of the maximum values of  $|m(t)|$  in Fig. 5, i.e.,  $|m(t)| < m_0$  except for  $t = 0$ . To underline this aspect further, Fig. 9 displays the energy in the course of the switching measured by the expectation value of  $\mathcal{H}_0$ ,

$$E(t) = N\{2S\lambda + 2S^2 - \langle a_i a_j \rangle \langle a_i^\dagger a_j^\dagger \rangle - \langle b_i b_j \rangle \langle b_i^\dagger b_j^\dagger \rangle - \chi(\langle b_i b_j \rangle \langle a_i^\dagger a_j^\dagger \rangle + \langle b_i^\dagger b_j^\dagger \rangle \langle a_i a_j \rangle)\}. \quad (32)$$

The dynamics of the energy relative to the energy of the initial state  $E_0(t) := E(t) - E(0)$  is depicted in Fig. 9 in the time interval  $t \in [0, \pi/J]$  for various degrees of anisotropy  $\chi \in [0.8, 0.99]$ . The magnetic field was chosen relatively high at  $h = 2J$  so that a rotation is possible for all anisotropies in the studied range.

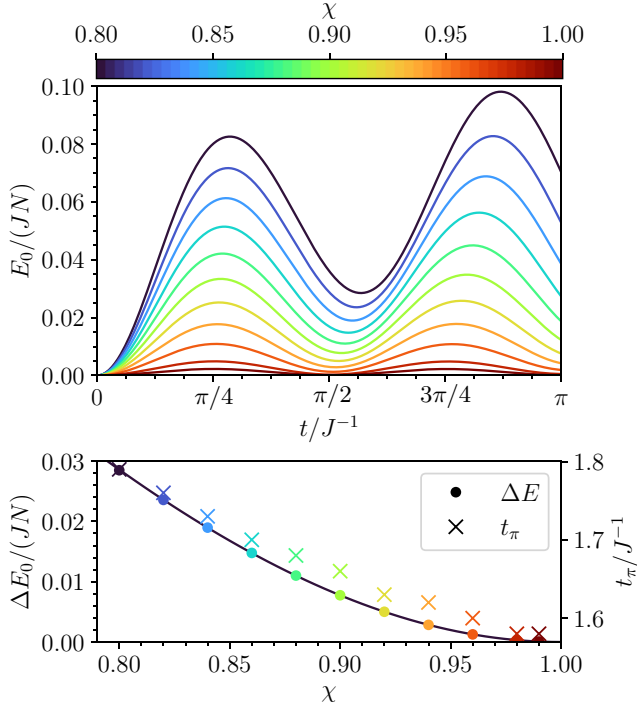


FIG. 9. In the upper panel, the temporal evolution of the energy  $E_0$  per lattice site is shown for an external field  $h = 2J$  and various anisotropies  $\chi \in [0.8, 0.99]$ . The color bar indicates the value of the anisotropy. The energy minima  $\Delta E_0$  show the energy after switching the magnetization by  $180^\circ$ ; they are not zero but indicate an energy increase because the switching does not lead to the degenerate ground state with magnetization  $-m_0$ . The energy increase after switching as well as the switching duration  $t_\pi$  are plotted against the anisotropy in the lower panel. The solid line results from a parabolic fit of the energy increase.

As expected, there is an energy minimum after switching since at this instant of time the switched state is closest to the other ground state with magnetization  $-m_0$ . In the isotropic case  $\chi = 1$ , the first minimum is reached at time  $t = \pi/(2J)$  according to Eq. (24). However, as already seen in Fig. 5, the switching duration increases and the minimum shifts to larger times upon increasing anisotropy (lowering of  $\chi$ ). It is obvious that the energy of the initial state is not reached again so that the overall energy is higher after switching the sublattice magnetization for  $\chi < 1$ . This underlines the effect of the many contributing spin modes that dephase and thereby depart from the initial coherent ground state. While this finding is physically plausible, we stress that we are not aware of other approaches displaying this feature prior to the time-dependent Schwinger boson approach advocated here.

The lower plot in Fig. 9 shows the increase in energy  $\Delta E_0$  after switching and the time  $t_\pi$  at which the energy minimum is reached as a function of  $\chi$ . The data points for  $\Delta E_0$  can be approximated to high accuracy by a parabola

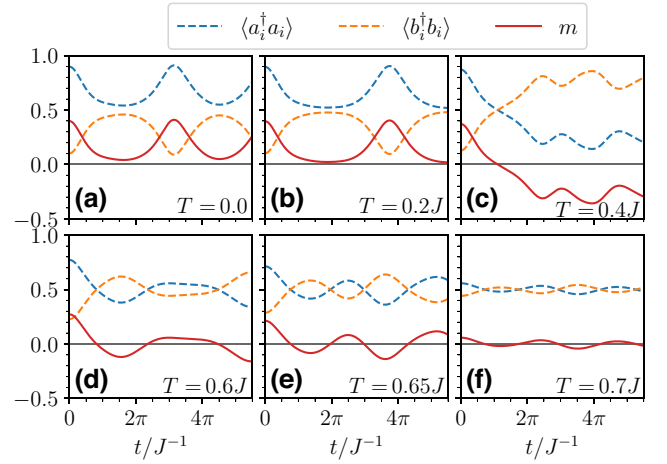


FIG. 10. Same as Fig. 5, but at various temperatures [panel (a) at  $T = 0$ , panel (b) at  $T = 0.2J$ , panel (c) at  $T = 0.4J$ , panel (d) at  $T = 0.6J$ , panel (e) at  $T = 0.65J$ , and panel (f) at  $T = 0.7J$ ] below the Néel temperature  $T_N = 0.704J$  for  $\chi = 0.9$ ,  $h = 0.86J$ , and  $L = 200$ .

$\Delta E_0(\chi) = c_0(1 - \chi^2)^m$  with parameters

$$c_0 = (0.230 \pm 0.002)J, \quad m = 2.04 \pm 0.05. \quad (33)$$

The switching times also increase steadily with growing anisotropy, but they do not evolve completely smoothly in our simulation, especially for  $\chi \rightarrow 1$ . This is to be attributed to the finite discretization used in the numerical computations.

## B. Switching at finite temperature

So far, we have studied the conditions for switching the magnetization at zero temperature. But the effect of finite temperature is highly relevant for two reasons. First, having applications in mind, a finite temperature must be accounted for because no setup will be operated at zero temperature. Second, temperature is a parameter that reduces the effective spin gap and makes the ordered system less robust and thus easier to switch. For this reason, a study of finite temperatures is in order.

Figure 10 shows the effect of finite temperature for an exemplary set of parameters. Clearly, no switching is possible at zero and at low temperatures. But, for intermediate temperatures  $T \gtrsim 0.4J$ , at least one swap  $m_0 \rightarrow -m_0$  is possible. Approaching the Néel temperature switching becomes possible even multiple times. Of course, the switched sublattice magnetization is reduced in its absolute value upon approaching  $T_N$ . But it can still be manipulated.

This is indeed a very promising observation because it suggests that temporary heating of the system up to the vicinity of the critical temperature, while still staying below it, facilitates the writing process of information into

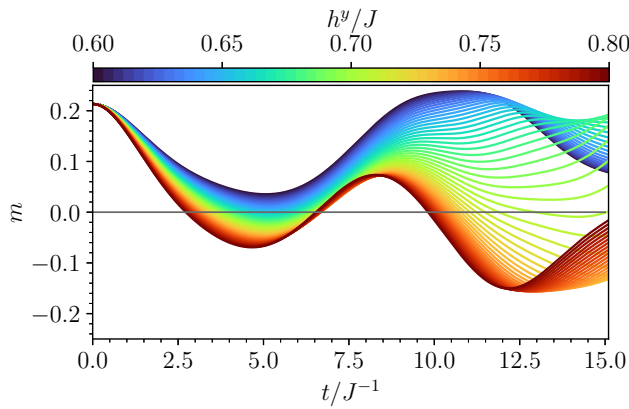


FIG. 11. Time evolution of the magnetization  $m$  for various external fields  $h^y \in [0.6J, 0.8J]$  at anisotropy  $\chi = 0.9$  and temperature  $T = 0.65J$  below  $T_N$ . The color bar at the top indicates the external field. We determine the threshold value  $h_t$  from the magnetic field at which the first minimum of  $m(t)$  touches  $m = 0$ .

a long-range ordered magnetic system. For long-time storage, the temperature can be lowered again after the writing process. Of course, heating the total system is not practical because it takes very long and the information content of adjacent domains risks getting lost. But one can envision that a short and focused laser pulse heats up the nanoscale region that one intends to switch. On the nanoscale, thermal diffusion will cool the manipulated domain quickly after the switching.

Hence, we investigate the finite-temperature case further. Figure 11 displays the temporal evolution of  $m(t)$  for various applied magnetic fields for a generic set of anisotropy and temperature. The phenomenology is similar, but not identical to that at zero temperature; cf. Fig. 6. At zero temperature, the switched curves appear to be mirror images of the nonswitched curves flipped around  $m = 0$ . At finite temperature, it is mostly the first minimum of  $m(t)$  that decreases further and further upon increasing the control field  $h^y$ . No clear point of inflection occurs except at very low temperatures (not shown). Hence, we here take the occurrence of a negative value of  $m(t)$  as a signature of switching, i.e., the threshold field  $h_t$  is determined from the field at which the first minimum touches the  $m = 0$  line. We point out that the threshold field determined in such a way can depend on the considered time interval (see also below), in particular if the instant in time at which the magnetization switches sign jumps as a function of the applied field. We analyzed the time interval  $t \in [0, 15/h^y]$ , i.e., for low values of the field, we scanned large intervals. Studying even larger intervals can only lower the values for  $h_t$  so that our values are at least rigorous upper bounds.

Next, it is important to track the threshold fields for various temperatures to learn how far they can be reduced by increasing the temperature up to  $T_N$ . Since the greatest effects occur close to the Néel temperatures, we do not

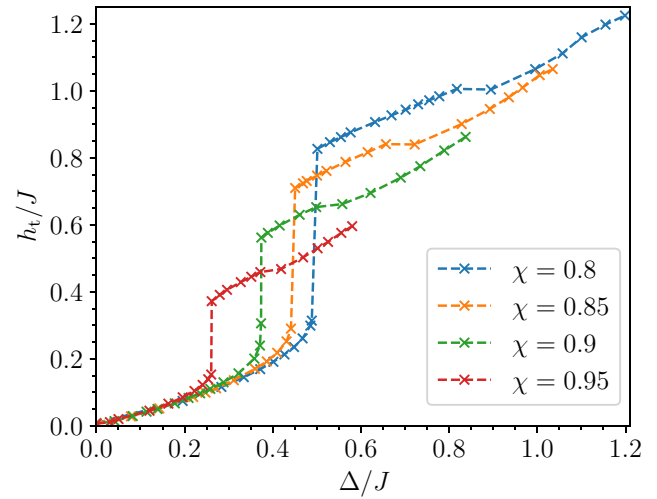


FIG. 12. Threshold magnetic field  $h_t$  versus the effective spin gap  $\Delta$  for various anisotropies. Note that  $\Delta$  vanishes as  $T \rightarrow T_N$ ; cf. Fig. 2(b). The data are obtained for a system size  $L = 200$ . The jump occurs for  $\chi = 0.95$  at  $T = 0.6215J$  with  $T_N = 0.652J$ , for  $\chi = 0.9$  at  $T = 0.6775J$  with  $T_N = 0.704J$ , for  $\chi = 0.85$  at  $T = 0.7065J$  with  $T_N = 0.725J$ , and for  $\chi = 0.8$  at  $T = 0.7225J$  with  $T_N = 0.732J$ .

plot the threshold fields as a function of  $T$ , but as a function of the effective spin gap  $\Delta$  in Fig. 12. We stress that there is a monotonic one-to-one mapping between the temperature and  $\Delta$ ; see Fig. 2(b). Clearly, the data support the finding that the threshold field  $h_t$  decreases, reducing the effective spin gap by increasing the temperature to the Néel temperature. But the almost quantitative agreement between the threshold field and spin gap we found at zero temperature (see Fig. 8) does not hold anymore. It would have meant that Fig. 12 displayed two straight lines through the origin with identical slopes of one. But the intriguing feature lies in the vanishing of the threshold field for  $T \rightarrow T_N$ . For application purposes, we conclude that increasing the temperature close to  $T_N$  can help significantly to switch the magnetization. Hence, one may envision that writing magnetic data is done at elevated temperatures realized by a short and locally focused laser pulse, while the long-time storage is done at low temperatures where the sublattice magnetization is considerably more robust.

A truly unexpected feature is the discontinuous jump at an intermediate value of the spin gap. It appears to be generic since it occurs for all anisotropies studied. Below the jump only fairly small fields are required to switch the magnetization. In view of this discontinuity, the imminent next question concerns its origin. To this end, we show in Fig. 13 the full temporal evolution of  $m(t)$  for two temperatures: one is just below the jump, i.e., with an effective spin gap  $\Delta$  slightly larger than the value at the jump, and the other temperature just above the jump, i.e., with an effective spin gap slightly smaller than the jump value.

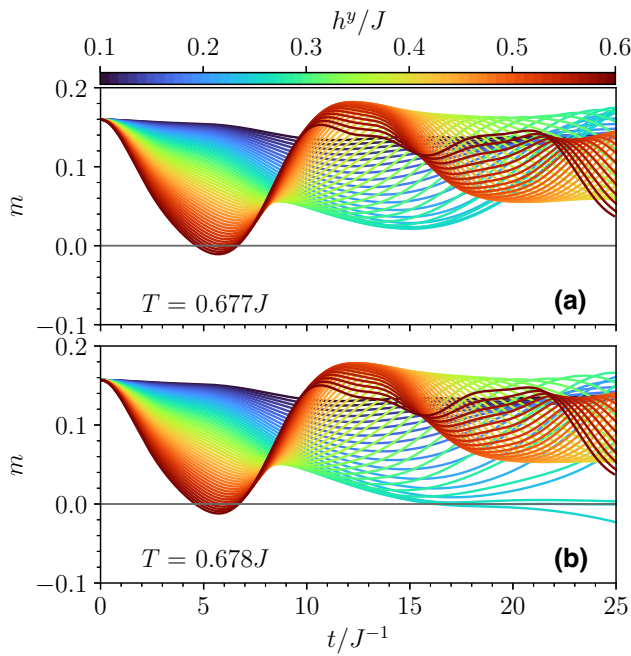


FIG. 13. Both panels show the full temporal evolution  $m(t)$  for  $\chi = 0.9$  for two very close values of the temperature of which one is just below [panel (a)] the temperature where the jump of  $h_t$  occurs and the other just above [panel (b)]. There is a sign change in  $m(t)$  in panel (a) at around  $t \approx 6J^{-1}$  for larger fields. But note the additional change of sign in  $m(t)$  in panel (b) at a larger time  $t \approx 17J^{-1}$  for lower fields. This is responsible for a sudden change in the threshold field.

Both panels show successful switching for some magnetic fields. But, for the lower temperature (larger  $\Delta$ ), the magnetization only switches for large fields at times  $t \approx 6J^{-1}$ . For the larger temperature (smaller  $\Delta$ ), the magnetization also switches for low fields at times  $t \approx 17J^{-1}$ . At these times, the lower temperature does not yet allow for a sign change of the magnetization. Thus, the jump in the instant in time, at which switching can be detected, explains in turn the jump in the threshold fields.

## V. CONCLUSIONS

Controlling the magnetization of long-range ordered quantum magnets is a key element in data storage in nanoscale domains. The magnetization orientation in such a domain serves as a bit. So far, it is realized and employed for ferromagnets. But it is established that quantum antiferromagnets display important advantages. They do not have stray fields that oppose close packing of the domains of magnetization, i.e., the bits. In addition, the generic time scales are shorter by 3 orders of magnitude in comparison to generic ferromagnets.

For these reasons, we investigated the switching of the antiferromagnetic sublattice magnetization in an anisotropic easy-axis Heisenberg antiferromagnet. We

aimed at the development of a suitable microscopic quantum approach to describe this phenomenon. For simplicity, we studied the model on a square lattice. The aim was to go beyond the description of the magnetizations on the two sublattices by two classical vectors (vector model). We intended to base our approach on a quantum model that captures all leading quantum and thermal effects. Such a model has to comprise all the magnetic modes, i.e., a spin-wave description was required. Addressing all modes allows one to deal with dephasing of the modes in the course of switching as well as with finite-temperature effects. These important effects are missed otherwise.

But the showstopper of conventional spin-wave theories is that they only capture the fluctuations around one of the degenerate ground states. Yet, for the purpose of switching from one ground state (up-down on sublattices A–B) to the other (down-up), this is obviously not sufficient. Hence we resorted to the Schwinger boson description that captures all degenerate ordered states as well as the disordered ones. We use the established mean-field description that reproduces the result of the usual self-consistent spin-wave theories in equilibrium based on the Holstein-Primakoff or the Dyson-Maleev representations. We stress that the Schwinger mean-field approach reaches about 30% accuracy even far away from the ground states, as can be estimated from the agreement of the Néel temperature in the Ising limit with the rigorous Onsager result [35].

Furthermore, we computed the spin gap within the Schwinger mean-field theory [18] and found results that agree with the reliable results from other techniques if the mean-field gap is scaled down by a factor of approximately 1.3. This is a very satisfying result in view of the simplicity of the mean-field approach and the low dimensionality of the system.

Using the equilibrium expectation values as starting values, we computed solutions of the Heisenberg equations of motions for the expectation values. In particular, we calculated the temporal evolution  $m(t)$  upon application of a uniform transverse magnetic field that induces a Larmor precession. The magnetization in the isotropic model is rotated without loss of coherence and for arbitrarily weak fields. In the anisotropic case, however, an activation energy needs to be overcome. For weak magnetic fields  $h$ , no switching is possible; only weak oscillations below the equilibrium magnetization are induced. Above a threshold value  $h_t$  switching is possible, but the coherence of all the involved magnetic modes is deteriorating. Thus, for fields just above the threshold, only a single switching is possible, while for large control fields, several swaps  $m_0 \leftrightarrow -m_0$  can be realized. The threshold fields  $h_t$  at zero temperature agree almost quantitatively with the spin gap. The larger the spin gap, the more robust the magnetic order. We stress that the necessity of a minimum field to overcome anisotropic energy barriers was known from classical two-vector descriptions. Our results confirm it in

an approach including the leading thermal and quantum fluctuations. But the dephasing of the momentum-resolved magnetic modes represents a feature that may have been expected on the basis of qualitative arguments, but only the Schwinger boson approach puts it on a quantitative basis.

Analyzing the time  $t_\pi$  needed to perform (or to fail) a swap displays a logarithmic divergence at the threshold value, both from above and from below. This behavior coincides precisely with the time needed for a massive particle to overcome an energy barrier. This means that the antiferromagnetic magnetization disposes of an inertia in its dynamics, as was observed both experimentally and theoretically in a classical vector model before [13].

Upon increasing the temperature, the equilibrium magnetization and the effective spin gap decrease towards the Néel temperature where both vanish. Thus, it is not surprising that the threshold magnetic field required for switching decreases upon increasing temperature and also vanishes at  $T_N$ . Our model including the leading quantum and thermal effects confirms this expectation beyond qualitative arguments in a quantitative calculation. The relation between temperature or, equivalently, the effective spin gap and the threshold field is monotonic. Unexpectedly, however, we found a discontinuity in the threshold fields. At an intermediate value of the effective spin gap  $\Delta$ , the required minimum field suddenly decreases by a finite amount. Because of the square root laws  $\Delta \propto \sqrt{T_N - T}$ , this spin-gap value corresponds to temperatures that are close to the transition temperature  $T_N$ . We could trace the origin of the jump to the full temporal evolution of the magnetization  $m(t)$  during the switching. The instant of time where  $m(t)$  changes sign jumps as well to longer times for lower fields.

What is the implication for experiment? As pointed out above, many parameters need to be taken into account. If we assume that  $J = 10$  meV and a small anisotropy  $\chi \approx 0.99$  and/or a temperature rather close to the Néel temperature, the threshold field corresponds roughly to  $0.05J = 0.5$  meV, which corresponds for  $g = 2$  to about 5 T. Note that the spin gaps and thus the threshold fields are likely to be 30% lower than the mean-field approach predicts. This is still a large field, but it is certainly realizable in a laboratory. Hence, we think that our results provide an interesting and quantitative guideline for future experiments. According to our findings, the temperature dependence of the switching merits close inspection in particular. In real material, we expect that there are further interactions to be included, for instance spin-phonon couplings. We expect that these additional interactions will enhance the dephasing in the course of the switching because the lattice degrees of freedom will also be involved and become excited.

The theoretical outlook comprises a large scope of promising extensions. Ferromagnets with nonrelativistic, parabolic magnon dispersion [18,23,26,27] can be addressed. Furthermore, the present calculation for

antiferromagnets can be extended to three dimensions and also to many other lattices. Certainly, other bipartite lattices can be treated in the very same fashion, but also frustrated lattices displaying long-range order such as the triangular lattice [36] can be tackled. One can also apply the approach to models with anisotropies such as single-ion anisotropies or anisotropies beyond easy axis, for instance with a fourfold rotation symmetry of the magnetizations. Furthermore, time-dependent control fields can be considered as well so that a plethora of fundamentally interesting as well as practically relevant issues, such as the influence of nanostructured confinement, are open for further investigation using the approach advocated here.

## ACKNOWLEDGMENTS

We thank Davide Bossini for drawing our attention to this topic and Christoph Lange for very useful discussions. We gratefully acknowledge financial support by the German Research Foundation (DFG) in project UH 90-14/1 (GSU) and in TRR 160 (AK). Furthermore, K.B. thanks the Studienstiftung des Deutschen Volkes for funding. We acknowledge financial support by DFG and TU Dortmund University within the funding programme Open Access Costs.

## APPENDIX A: SOLVING THE SCHWINGER BOSON MEAN-FIELD HAMILTONIAN IN EQUILIBRIUM

Here we provide the steps towards solving the Schwinger boson mean-field problem at equilibrium in the isotropic and the anisotropic cases. We address the case at zero temperature mainly, but also provide exemplary dispersions at finite temperature.

### 1. Isotropic case

Calculating the Fourier transformation of the Hamiltonian is the first step towards diagonalization:

$$\mathcal{H} = E_{\text{MF}} + \sum_{\mathbf{k}} \{ \lambda (a_{\mathbf{k}}^\dagger a_{\mathbf{k}} + b_{\mathbf{k}}^\dagger b_{\mathbf{k}}) - A \gamma_{\mathbf{k}} (a_{\mathbf{k}} a_{-\mathbf{k}} + b_{\mathbf{k}} b_{-\mathbf{k}} + \text{H.c.}) \}. \quad (\text{A1})$$

Here  $\gamma_{\mathbf{k}} := \frac{1}{2} (\cos(k_x) + \cos(k_y))$ , where we set the lattice constant to unity. The sum refers to the entire Brillouin zone since the Schwinger bosons are not restricted to one sublattice. Next, standard Bogoliubov transformations for both the  $a$  and  $b$  bosons,

$$a_{\mathbf{k}}^\dagger = \cosh(\theta_{\mathbf{k}}) \alpha_{\mathbf{k}}^\dagger + \sinh(\theta_{\mathbf{k}}) \alpha_{-\mathbf{k}}, \quad (\text{A2a})$$

$$b_{\mathbf{k}}^\dagger = \cosh(\theta_{\mathbf{k}}) \beta_{\mathbf{k}}^\dagger + \sinh(\theta_{\mathbf{k}}) \beta_{-\mathbf{k}}, \quad (\text{A2b})$$

and the corresponding Hermitian conjugate relations lead to the diagonalized Hamiltonian

$$\mathcal{H} = E_{\text{MF}} - N\lambda + \sum_{\mathbf{k}} \omega_{\mathbf{k}}^{\text{iso}} (\alpha_{\mathbf{k}}^\dagger \alpha_{\mathbf{k}} + \beta_{\mathbf{k}}^\dagger \beta_{\mathbf{k}} + 1), \quad (\text{A3})$$

where we have chosen  $\lambda \tanh(2\theta_{\mathbf{k}}) = 2A\gamma_{\mathbf{k}}$ . The resulting dispersion reads

$$\omega_{\mathbf{k}}^{\text{iso}} = \sqrt{\lambda^2 - (2A\gamma_{\mathbf{k}})^2}. \quad (\text{A4})$$

The value  $\lambda$  results from the condition that Eq. (8) holds on average, i.e., for the expectation values of the particle numbers. The expectation value  $A$  is defined in Eq. (14), yielding

$$A = \frac{1}{N} \sum_{\mathbf{k}} \frac{2A\gamma_{\mathbf{k}}^2}{\omega_{\mathbf{k}}^{\text{iso}}} \coth(\beta\omega_{\mathbf{k}}^{\text{iso}}/2), \quad (\text{A5a})$$

$$2S + 1 = \frac{1}{N} \sum_{\mathbf{k}} \frac{\lambda}{\omega_{\mathbf{k}}^{\text{iso}}} \coth(\beta\omega_{\mathbf{k}}^{\text{iso}}/2). \quad (\text{A5b})$$

Here,  $\beta$  is the inverse temperature up to Boltzmann's constant. Solving these equations requires finding a non-linear zero depending on two variables. For finite systems  $N < \infty$  or for finite temperature, it can be tackled by direct numerics. No finite sublattice magnetization occurs because no finite system displays long-range antiferromagnetic order. The same holds for the infinite two-dimensional isotropic system at finite temperature according to the Mermin-Wagner theorem [34].

Spontaneous long-range order in the infinite system at zero temperature appears as Bose-Einstein condensation [18,23,24]. The Goldstone theorem [18] tells us that the spectrum must be gapless; thus,  $\lambda = A$  holds. Then we encounter singularities at  $\mathbf{k} = \mathbf{0}$  and  $\mathbf{k} = (\pi, \pi)$  for finite  $N$ . In the thermodynamic limit  $N \rightarrow \infty$ , the sums in Eqs. (A5) do not converge uniformly to integrals. For any finite  $N$ , the spectrum is *not* gapless, but displays a small finite-size gap  $\Delta_N$ . Although this gap vanishes for  $N \rightarrow \infty$ , a contribution from the points  $\mathbf{k} = \mathbf{0}$  and  $\mathbf{k} = (\pi, \pi)$  remains. Concretely, we set  $\lambda^2 = (2A)^2(1 + \kappa^2)$  with  $\kappa = f/N$ , implying that  $\omega_{\mathbf{k}}^{\text{iso}} = 2A\sqrt{1 + \kappa^2 - \gamma_{\mathbf{k}}^2}$ . Then the limit  $N \rightarrow \infty$  is performed for Eqs. (A5) and we obtain

$$A = \frac{1}{4\pi^2} \int_{\text{BZ}} dk^2 \frac{\gamma_{\mathbf{k}}^2}{\sqrt{1 - \gamma_{\mathbf{k}}^2}} + \frac{2}{f}, \quad (\text{A6a})$$

$$2S + 1 = \frac{1}{4\pi^2} \int_{\text{BZ}} dk^2 \frac{1}{\sqrt{1 - \gamma_{\mathbf{k}}^2}} + \frac{2}{f}. \quad (\text{A6b})$$

This contribution from single points in the Brillouin zone stands for the macroscopic contribution of a few modes

[here precisely four modes,  $\alpha_{\mathbf{k}}, \beta_{\mathbf{k}}$  at  $\mathbf{k} = \mathbf{0}$  and  $(\pi, \pi)$ ], representing a Bose-Einstein condensation. The sublattice magnetization per site  $m_0 = |\langle S_i^z \rangle|$  in the ordered phase is given by [18]

$$\begin{aligned} m_0 &= 1/f \\ &= S + \frac{1}{2} - \frac{1}{8\pi^2} \int_{\text{BZ}} dk^2 \frac{1}{\sqrt{1 - \gamma_{\mathbf{k}}^2}}. \end{aligned} \quad (\text{A7})$$

Subtracting Eq. (A6a) from Eq. (A6b) yields

$$2S + 1 - A = \frac{1}{4\pi^2} \int_{\text{BZ}} dk^2 \sqrt{1 - \gamma_{\mathbf{k}}^2} =: 2\delta + 1 \quad (\text{A8a})$$

$$\iff A = 2(S - \delta), \quad (\text{A8b})$$

$$2\delta = -0.15795, \quad (\text{A8c})$$

$$\omega_{\mathbf{k}}^{\text{iso}} = 4(S - \delta)\sqrt{1 - \gamma_{\mathbf{k}}^2}, \quad (\text{A8d})$$

where  $2\delta$  is computed numerically.

In Fig. 14, we show the resulting dispersion in the thermodynamic limit (black line) and for an arbitrary finite  $\kappa = 0.2J$  (blue dashed line) for illustration. Note that the black line shows the dispersion of both the  $\alpha$  and the  $\beta$  bosons because they are degenerate. Since the spin operators consist of bilinear bosonic expressions [see Eqs. (6)], a physical excitation, i.e., the magnon, will not consist of a single  $\alpha$  or  $\beta$  particle. Given, however, the macroscopic occupations at  $\mathbf{k} = \mathbf{0}$  and  $(\pi, \pi)$ , it is justified to replace the bosonic operators at these wave vectors according to

$$\alpha_{\mathbf{k}} \rightarrow \langle \alpha_{\mathbf{k}} \rangle = \sqrt{Nm_0/4}, \quad (\text{A9a})$$

$$\beta_{\mathbf{k}} \rightarrow \langle \beta_{\mathbf{k}} \rangle = \sqrt{Nm_0/4}, \quad (\text{A9b})$$

if no spontaneous symmetry breaking is accounted for. In the ordered phase, only one of the bosons displays the macroscopic occupation, so that either  $\alpha_{\mathbf{k}} \rightarrow \sqrt{Nm_0/2}$  or  $\beta_{\mathbf{k}} \rightarrow \sqrt{Nm_0/2}$  holds at  $\mathbf{k} = \mathbf{0}$  and  $(\pi, \pi)$ ; see Ref. [18]. With these substitutions, the creation of a magnon is described by  $\sqrt{Nm_0/2}\beta_{\mathbf{k}}^\dagger$  if the  $\alpha$  bosons condense and by  $\sqrt{Nm_0/2}\alpha_{\mathbf{k}}^\dagger$  if the  $\beta$  bosons condense. The dispersion from the Schwinger boson mean-field theory is identical to the self-consistent spin-wave theory resulting from a  $1/S$  expansion in the Holstein-Primakoff and Dyson-Maleev representations up to and including order  $1/S$ .

Later we compute solutions for the self-consistency conditions numerically for finite clusters with  $N < \infty$  because we need them as initial conditions for switching processes. Rigorously, no spontaneous symmetry breaking takes place due to the finiteness of the sample size and thus no finite sublattice magnetization can be determined. As a remedy to approximate the thermodynamic, infinite lattice, we include a tiny symmetry-breaking alternating

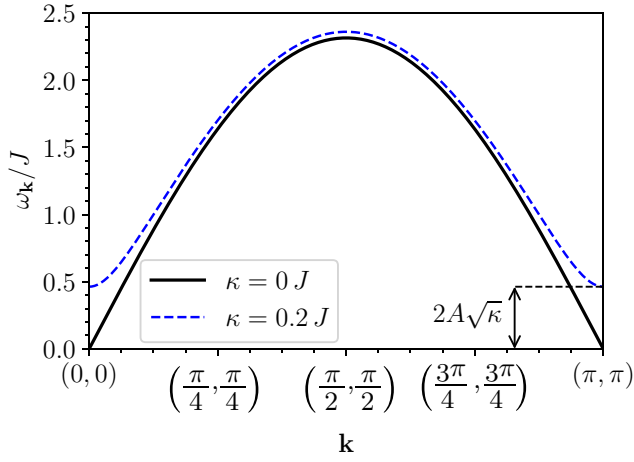


FIG. 14. The black line depicts the degenerate dispersion of the two Schwinger bosons in the long-range ordered isotropic case in the thermodynamic limit. The blue dashed line illustrates the dispersion, assuming a finite  $\kappa = 0.2J$ .

field  $h_{\text{alt}}^z \propto 1/N$  that reproduces the analytically known sublattice magnetization  $m_0 = S - 0.19660$ .

In order to determine a suitable value of the magnetic field, the initial magnetization  $m(h_{\text{alt}}^z)$  of the isotropic system for various system sizes and spin  $S = 1/2$  is plotted against the scaled field  $h_{\text{alt}}^z$  in Fig. 15. All curves demonstrate that a small field scaling  $\propto 1/N$  is already sufficient to generate the magnetic order. The larger the system, the more the magnetization curve converges to the discontinuous curve of an infinitely large system, where the magnetization persists even for  $h_{\text{alt}}^z \rightarrow 0^+$ . The inset shows that the sublattice magnetization  $m(h_{\text{alt}}^z)$  corresponds to the desired value  $m_{0,\text{iso}} = 0.3034$  for  $h_{\text{alt}}^z = 1.329 J N^{-1}$ . We find it remarkable and reassuring that in the close vicinity of this value, the curves for various  $L$  almost intersect. They do not intersect precisely in one point, but in a very narrow region. Still, this corroborates the advocated way to approximate the thermodynamic limit by finite clusters.

## 2. Anisotropic case

For diagonalization, we proceed as in the isotropic case. After Fourier transformation, the Hamiltonian is given by

$$\begin{aligned} \mathcal{H} = & E_{\text{MF}} + \lambda \sum_{\mathbf{k}} (a_{\mathbf{k}}^\dagger a_{\mathbf{k}} + b_{\mathbf{k}}^\dagger b_{\mathbf{k}}) \\ & - \frac{1}{2} \sum_{\mathbf{k}} \gamma_{\mathbf{k}} \{ A(1 + \chi)(a_{\mathbf{k}} a_{-\mathbf{k}} + b_{\mathbf{k}} b_{-\mathbf{k}} + \text{H.c.}) \\ & + B(1 - \chi)(a_{\mathbf{k}} a_{-\mathbf{k}} - b_{\mathbf{k}} b_{-\mathbf{k}} + \text{H.c.}) \}. \end{aligned} \quad (\text{A10})$$

Since the nondiagonal Bogoliubov terms of the two Schwinger bosons flavors have different prefactors, it is no longer possible to use the same Bogoliubov angles in the

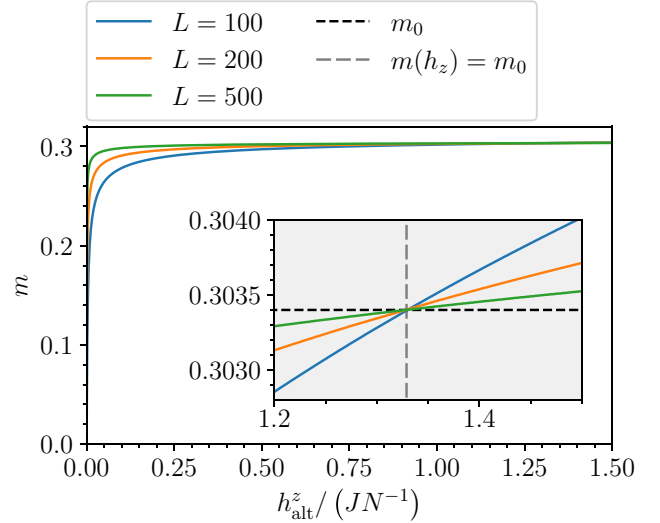


FIG. 15. The initial magnetization  $m$  of the isotropic system, i.e.,  $\chi = 1$ , as a function of a small field  $h_{\text{alt}}^z$  for different system sizes. Magnetic order is already obtained for small fields; recall that  $N = L^2$ . The desired initial magnetization  $m_{0,\text{iso}} = 0.3034$  is reached for  $h_{\text{alt}}^z = 1.329 J N^{-1}$ , as shown in the inset. Around this value, the curves for the various system sizes intersect.

transformations. Instead, we use

$$a_{\mathbf{k}}^\dagger = \cosh(\theta_{\mathbf{k}}^a) \alpha_{\mathbf{k}}^\dagger + \sinh(\theta_{\mathbf{k}}^a) \alpha_{-\mathbf{k}}, \quad (\text{A11a})$$

$$b_{\mathbf{k}}^\dagger = \cosh(\theta_{\mathbf{k}}^b) \beta_{\mathbf{k}}^\dagger + \sinh(\theta_{\mathbf{k}}^b) \beta_{-\mathbf{k}}, \quad (\text{A11b})$$

and the Hermitian conjugate operators using the condition

$$\gamma_{\mathbf{k}} = \frac{\lambda}{C_-} \tanh(2\theta_{\mathbf{k}}^a) = \frac{\lambda}{C_+} \tanh(2\theta_{\mathbf{k}}^b) \quad (\text{A12})$$

with  $C_{\pm}$  defined in Eq. (18). In this way, we obtain the diagonal form

$$\begin{aligned} \mathcal{H} = & E_{\text{MF}} - N\lambda + \sum_{\mathbf{k}} \left\{ \omega_{\mathbf{k}}^- \left( \alpha_{\mathbf{k}}^\dagger \alpha_{\mathbf{k}} + \frac{1}{2} \right) \right. \\ & \left. + \omega_{\mathbf{k}}^+ \left( \beta_{\mathbf{k}}^\dagger \beta_{\mathbf{k}} + \frac{1}{2} \right) \right\}. \end{aligned} \quad (\text{A13})$$

Concomitantly, there are two different spin-wave dispersions

$$\omega_{\mathbf{k}}^{\pm} = \sqrt{\lambda^2 - C_{\pm}^2 \gamma_{\mathbf{k}}^2}. \quad (\text{A14})$$

For  $\chi = 1$ , the two dispersions coincide and reproduce the isotropic dispersion (A4).

Physically, a spin gap is expected to result from the anisotropy reducing the continuous symmetry to a discrete  $\mathbb{Z}_2$  symmetry. Therefore, spontaneous symmetry breaking

due to the magnetic order no longer breaks a continuous symmetry and no massless Goldstone bosons need to occur. Still, the Schwinger boson description of the ordered phase requires a condensation of one Schwinger boson flavor at zero temperature. Let us assume that the  $\alpha$  bosons condense so that their dispersion is gapless in the thermodynamic limit at  $T = 0$ . We stress that this does not imply that the physical excitations are gapless because they imply the annihilation of an  $\alpha$  boson combined with the creation of a  $\beta$  boson.

We need to derive the conditions for the parameters  $A$ ,  $B$ , and  $\lambda$  to make any quantitative statements. The constraint and the expectation values  $A$  and  $B$  yield

$$2S = \frac{\lambda}{2N} \sum_{\mathbf{k}} \left[ \frac{\coth(\beta\omega_{\mathbf{k}}^-/2)}{\omega_{\mathbf{k}}^-} + \frac{\coth(\beta\omega_{\mathbf{k}}^+/2)}{\omega_{\mathbf{k}}^+} \right] - 1, \quad (\text{A15a})$$

$$A = \frac{1}{2N} \sum_{\mathbf{k}} \gamma_{\mathbf{k}}^2 \left[ \frac{C_- \coth(\beta\omega_{\mathbf{k}}^-/2)}{\omega_{\mathbf{k}}^-} + \frac{C_+ \coth(\beta\omega_{\mathbf{k}}^+/2)}{\omega_{\mathbf{k}}^+} \right], \quad (\text{A15b})$$

$$B = \frac{1}{2N} \sum_{\mathbf{k}} \gamma_{\mathbf{k}}^2 \left[ \frac{C_- \coth(\beta\omega_{\mathbf{k}}^-/2)}{\omega_{\mathbf{k}}^-} - \frac{C_+ \coth(\beta\omega_{\mathbf{k}}^+/2)}{\omega_{\mathbf{k}}^+} \right]. \quad (\text{A15c})$$

These equations allow us to determine the dispersion at zero and at finite temperature. The case of zero temperature is again a bit subtle; the relevant treatment of the equations at  $T = 0$  is described below. The resulting dispersion is displayed in Fig. 16. Clearly, the spin gap in the physical dispersion appears and grows for larger anisotropy.

The behavior of the spin gap  $\Delta$  as a function of the anisotropy parameter  $\chi$  is of particular interest. The required input parameter is the product  $AB$ ; we point out how we compute it.

For the condensation of the  $\alpha$  bosons, the dispersion  $\omega^-$  should become gapless for an infinitely large system at zero temperature, which is why

$$\lambda^2 = C_-^2(1 + \kappa^2) \quad (\text{A16})$$

is chosen with  $\kappa = \tilde{f}/N$ . We use  $\tilde{f}$  because only one of the two boson flavors is to condense. As before, this yields the dispersions

$$\omega_{\mathbf{k}}^- = C_- \sqrt{1 + \kappa^2 - \gamma_{\mathbf{k}}^2}, \quad (\text{A17a})$$

$$\omega_{\mathbf{k}}^+ = \sqrt{C_-^2(1 + \kappa^2) - C_+^2 \gamma_{\mathbf{k}}^2}. \quad (\text{A17b})$$

It is important to note that only  $\omega_{\mathbf{k}}^+$  describes the true spin-wave spectrum for  $T = 0$  because the operator of the condensed boson can be replaced,  $\alpha_{\mathbf{k}}^{(\dagger)} \rightarrow \sqrt{Nm_0}/2$ . In the thermodynamic limit  $N \rightarrow \infty$ , the sums in Eqs. (A15)

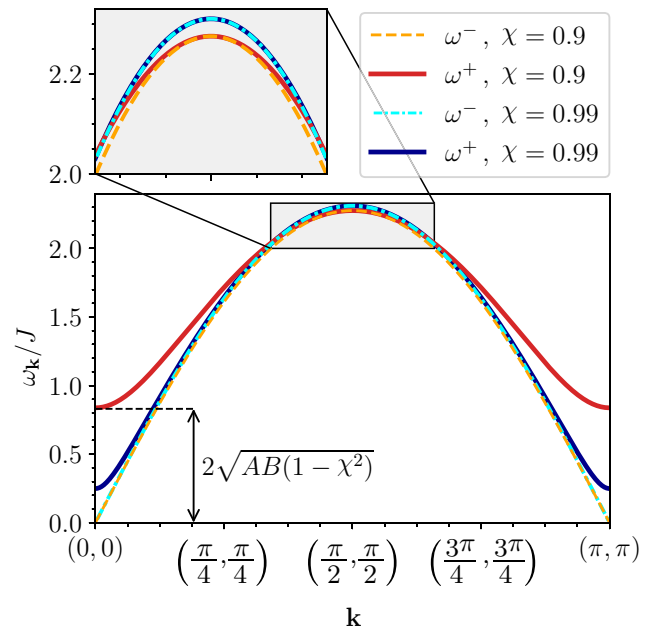


FIG. 16. Dispersions  $\omega_{\mathbf{k}}^{\pm}$  in an antiferromagnetic spin-1/2 square lattice at zero temperature, plotted exemplarily for the two anisotropies  $\chi = 0.9$  and  $\chi = 0.99$ . For the same  $\chi$ , the maxima of the dispersions  $\omega_{\mathbf{k}}^+$  and  $\omega_{\mathbf{k}}^-$  coincide, while  $\omega_{\mathbf{k}}^-$  is gapless and  $\omega_{\mathbf{k}}^+$  displays the physical energy gap at  $\mathbf{k} = (0, 0)$  and  $\mathbf{k} = (\pi, \pi)$ . Note that  $\omega_{\mathbf{k}}^-$  does not describe observable modes. As expected, the energy gap  $\Delta = 2\sqrt{AB(1 - \chi^2)}$  increases with increasing anisotropy, i.e., increasing deviation of  $\chi$  from 1.

become integrals as before plus the contributions from  $\mathbf{k} = (0, 0)$  and  $(\pi, \pi)$ :

$$2S = \frac{1}{8\pi^2} \int_{\text{BZ}} dk^2 \left[ \frac{1}{\sqrt{1 - \gamma_{\mathbf{k}}^2}} + \frac{C_-}{\sqrt{C_-^2 - C_+^2 \gamma_{\mathbf{k}}^2}} \right] + \frac{1}{\tilde{f}} - 1, \quad (\text{A18a})$$

$$A = \frac{1}{8\pi^2} \int_{\text{BZ}} dk^2 \gamma_{\mathbf{k}}^2 \left[ \frac{1}{\sqrt{1 - \gamma_{\mathbf{k}}^2}} + \frac{C_+}{\sqrt{C_-^2 - C_+^2 \gamma_{\mathbf{k}}^2}} \right] + \frac{1}{\tilde{f}}, \quad (\text{A18b})$$

$$B = \frac{1}{8\pi^2} \int_{\text{BZ}} dk^2 \gamma_{\mathbf{k}}^2 \left[ \frac{1}{\sqrt{1 - \gamma_{\mathbf{k}}^2}} - \frac{C_+}{\sqrt{C_-^2 - C_+^2 \gamma_{\mathbf{k}}^2}} \right] + \frac{1}{\tilde{f}}. \quad (\text{A18c})$$

Finally, Eqs. (A18b) and (A18c) are each subtracted from Eq. (A18a), yielding the two equations

$$2S + 1 - A = \frac{1}{8\pi^2} \int_{\text{BZ}} dk^2 \left[ \frac{1 - \gamma_{\mathbf{k}}^2}{\sqrt{1 - \gamma_{\mathbf{k}}^2}} + \frac{C_- - C_+ \gamma_{\mathbf{k}}^2}{\sqrt{C_-^2 - C_+^2 \gamma_{\mathbf{k}}^2}} \right], \quad (\text{A19a})$$

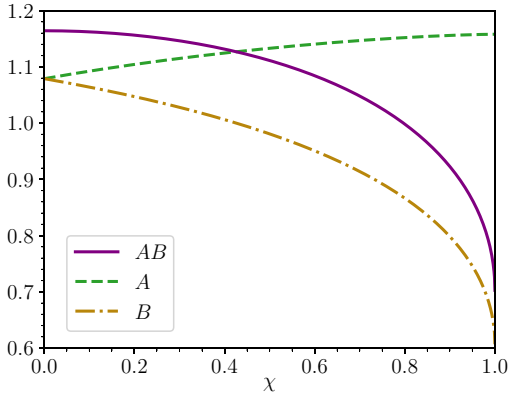


FIG. 17. Expectation values  $A$  and  $B$  and their product in equilibrium plotted as a function of the anisotropy  $\chi$ . These values enter in the determination of the spin gap in Fig. 1 and of the magnetization in Fig. 18.

$$2S + 1 - B = \frac{1}{8\pi^2} \int_{\text{BZ}} dk^2 \left[ \frac{1 - \gamma_{\mathbf{k}}^2}{\sqrt{1 - \gamma_{\mathbf{k}}^2}} + \frac{C_- + C_+ \gamma_{\mathbf{k}}^2}{\sqrt{C_-^2 - C_+^2 \gamma_{\mathbf{k}}^2}} \right]. \quad (\text{A19b})$$

These equations allow us to determine  $A$  and  $B$  and thus  $AB$ . The results are shown in Fig. 17. The expectation value  $A$  appears to be smooth, while  $B$  and thus the product  $AB$  display a singular behavior at  $\chi = 1$ . The Lagrange multiplier  $\lambda$  is implicitly fixed by the condition that the  $\alpha$  bosons condense and their dispersion is massless.

To determine the sublattice magnetization from Eq. (19), we consider its thermodynamic limit  $N \rightarrow \infty$ :

$$m_0 = \frac{1}{16\pi^2} \int_{\text{BZ}} dk^2 \left[ \frac{1}{\sqrt{1 - \gamma_{\mathbf{k}}^2}} - \frac{C_-}{\sqrt{C_-^2 - C_+^2 \gamma_{\mathbf{k}}^2}} \right] + \frac{1}{2\tilde{f}}. \quad (\text{A21})$$

Subtracting this equation from half the Eq. (A18a) yields

$$S + \frac{1}{2} - m_0 = \frac{1}{8\pi^2} \int_{\text{BZ}} dk^2 \frac{C_-}{\sqrt{C_-^2 - C_+^2 \gamma_{\mathbf{k}}^2}}, \quad (\text{A22})$$

eliminating the condensate contribution  $\propto 1/\tilde{f}$ . Solving the last equation for  $m_0$  yields Eq. (20). The explicit results are displayed in Fig. 18 as a function of  $\chi$  for  $S = 1/2$ . As expected, the magnetization approaches its maximum value  $S$  for  $\chi \rightarrow 0$  where the model becomes the Ising model.

For the anisotropic system, the ordered phase also persists at finite temperature. No Bose condensation occurs, but both flavors of Schwinger bosons are occupied and both their dispersions display gaps, as illustrated in Fig. 19. The effective physical gap  $\Delta$  is given by the difference  $\Delta^+ - \Delta^-$ ; see the main text.

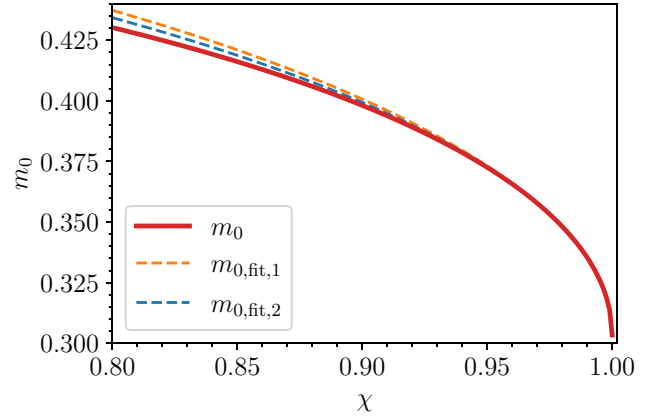


FIG. 18. The magnetization at zero temperature is shown as a function of the anisotropy parameter  $\chi$  according to Eq. (20) as a solid red line. The fit functions are  $m_{0,\text{fit},i} = m_{0,\text{iso}} + c_i(1 - \chi^2)_i^{\mu_i}$  with  $c_1 = (0.223 \pm 0.004)J$ ,  $\mu_1 = 1/2$  for the orange curve and  $c_2 = (0.215 \pm 0.005)J$ ,  $\mu_2 = 0.49 \pm 0.01$  for the blue curve.

## APPENDIX B: OVERCOMING A POTENTIAL BARRIER

Here we motivate by a classical example why a logarithmic singularity is to be expected in Fig. 7 and why this is an indication of inertia. For this purpose, a potential  $V(x) = -\frac{1}{2}\gamma^2 x^2$  is considered, as shown in Fig. 20. We want to know how long it takes a mass to move over this potential barrier. For the sake of simplicity, the mass is set to  $m = 1$ . The Hamilton function of the system reads

$$\mathcal{H} = \frac{p^2}{2} - \frac{1}{2}\gamma^2 x^2. \quad (\text{B1})$$

We highlight that the existence of the kinetic energy reflects the existence of inertia. The resulting equation of motion reads

$$\ddot{x} - \gamma^2 x = 0, \quad (\text{B2})$$

and has the general solution

$$x(t) = F \cosh(\gamma t) + G \sinh(\gamma t). \quad (\text{B3})$$

The initial conditions are  $x(0) = x_0 > 0$  and  $\dot{x}(0) = -v_0 < 0$ . Thus, we find that  $F = x_0$  and  $G = -v_0/\gamma$ . The total energy of the system takes the value

$$2E = v_0^2 - \gamma^2 x_0^2 = (\gamma G)^2 - (\gamma F)^2. \quad (\text{B4})$$

The marginal case is given for  $E = 0$  because in this case the kinetic energy disappears exactly when the potential maximum is reached. This corresponds to  $F = -G$ ,

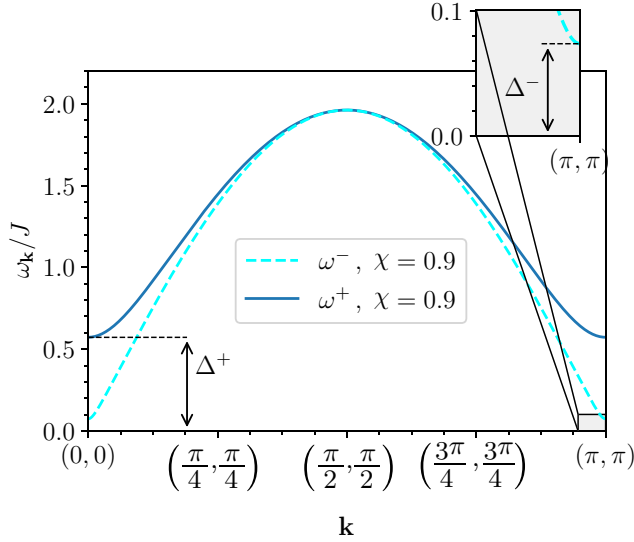


FIG. 19. Dispersions  $\omega_{\mathbf{k}}^{\pm}$  in an antiferromagnetic spin-1/2 square lattice at finite temperature, plotted exemplarily for  $\chi = 0.9$  at  $T = 0.65J$ .

implying that

$$x(t) = x_0(\cosh(\tau) - \sinh(\tau)) = x_0 e^{-\tau} \quad (\text{B5})$$

with  $\tau := \gamma t$ . Note that the solution  $F = G$  is discarded because of the restrictions  $F > 0$  and  $G < 0$ . The maximum at  $x = 0$  is thus reached exponentially slowly. Next, we consider a small deviation  $G = -x_0(1 + 2\delta)$  from the marginal case. For  $\delta > 0$ , the total energy is positive, and therefore the potential barrier can be passed. We calculate the necessary time when point  $-x_0$  is reached

$$-x_0 = x_0 e^{-\tau} - \delta x_0 (e^{\tau} - e^{-\tau}) \quad (\text{B6a})$$

$$\iff 0 = \delta(y^2 - 1) - y - 1 \quad \text{with } y := e^{\tau} \quad (\text{B6b})$$

$$\iff y = \frac{1}{2\delta} + \sqrt{\frac{1}{4\delta^2} + \frac{1+\delta}{\delta}} \\ = 1 + \frac{1}{\delta} + \mathcal{O}(\delta^2). \quad (\text{B6c})$$

The other solution of the quadratic equation is negative and therefore not a physical solution. The position  $-x_0$  is reached at time

$$\gamma t = \tau = -\ln|\delta| + \delta + \mathcal{O}(\delta^2). \quad (\text{B7})$$

For  $\delta < 0$ , the total energy is negative, and therefore the potential barrier cannot be passed; the passage fails. In this

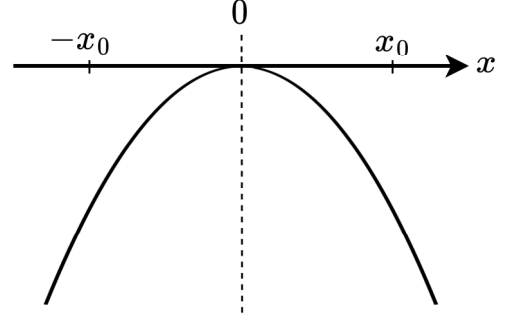


FIG. 20. The considered potential barrier  $V(x) = -\frac{1}{2}\gamma^2 x^2$ . The points  $\pm x_0$  are used to indicate whether the barrier has been overcome or not.

case, we calculate the time it takes to get back to point  $x_0$ :

$$x_0 = x_0 e^{-\tau} + |\delta|x_0(e^{\tau} - e^{-\tau}) \quad (\text{B8a})$$

$$\iff 0 = y - 1 - |\delta|(y^2 - 1) \quad (\text{B8b})$$

$$\iff y = \frac{1}{2|\delta|} + \sqrt{\frac{1}{4|\delta|^2} - \frac{1-|\delta|}{\delta}} \\ = \frac{1}{|\delta|} - 1 + \mathcal{O}(\delta^2). \quad (\text{B8c})$$

Again, the other solution of the quadratic equation is not physically significant. So the time for reaching  $x_0$  again is

$$\gamma t = \tau = -\ln|\delta| + \delta + \mathcal{O}(\delta^2). \quad (\text{B9})$$

Remarkably, the same result ensues for succeeding to pass the barrier as for failing to pass it. In both cases, a logarithmic divergence of the time occurs, just as we observed for switching the sublattice magnetization in Figs. 6 and 7. Note that the fitted prefactors in Eqs. (30) and (31) are very close to each other, as one expects from the classical calculation presented above. Note that this symmetry is perfectly reflected by the curves in Fig. 6 for magnetic fields just above and just below the threshold value that are mirror images of one another in the vicinity of the first extremum for  $t > 0$ .

In addition, we observe in solution (B5) as well as in the curves in Fig. 6 for the cases in the vicinity of the threshold that most of the time is spent around the energy maximum  $x \approx 0$  or  $m \approx 0$ , respectively. This underlines the conclusion that we are dealing with a process governed by inertia: what matters is the maximum energy that the switching term can provide. In contrast, a process without inertia, governed by friction, would spend most of the time close to the point where the maximum force is required. This is certainly not the case for  $m \approx 0$ , but rather would be around  $m \approx \pm m_0/2$ . Thus, the curves in Fig. 6 underline the conclusion that the magnetization dynamics in quantum antiferromagnets is governed by inertia.

- [1] L. F. Néel, Magnetism and the local molecular field—nobel lecture (1970), <https://www.nobelprize.org/prizes/physics/1970/nel/lecture/>.
- [2] P. K. Misra, *Physics of Condensed Matter* (Academic Press, Boston, 2011). 1st ed.
- [3] O. Gomonay, T. Jungwirth, and J. Sinova, Concepts of antiferromagnetic spintronics, *Phys. Status Solidi RRL* **11**, 1700022 (2017).
- [4] C. P. Chen and C. Zhang, Data-intensive applications, challenges, techniques and technologies: A survey on big data, *Inf. Sci. (NY)* **275**, 314 (2014).
- [5] M. Hilbert and P. López, The world's technological capacity to store, communicate, and compute information, *Science* **332**, 60 (2011).
- [6] S. Loth, S. Baumann, C. P. Lutz, D. M. Eigler, and A. J. Heinrich, Bistability in atomic-scale antiferromagnets, *Science* **335**, 196 (2012).
- [7] E. V. Gomonay and V. M. Loktev, Spintronics of antiferromagnetic systems (review article), *Low Temp. Phys.* **40**, 17 (2014).
- [8] T. Kampfrath, A. Sell, G. Klatt, A. Pashkin, S. Mährlein, T. Dekorsy, M. Wolf, M. Fiebig, A. Leitenstorfer, and R. Huber, Coherent terahertz control of antiferromagnetic spin waves, *Nat. Photonics* **5**, 31 (2011).
- [9] T. Jungwirth, X. Marti, P. Wadley, and J. Wunderlich, Antiferromagnetic spintronics, *Nat. Nanotechnol.* **11**, 231 (2016).
- [10] L. Baldrati, A. Ross, T. Niizeki, C. Schneider, R. Ramos, J. Cramer, O. Gomonay, M. Filianina, T. Savchenko, D. Heinze, A. Kleibert, E. Saitoh, J. Sinova, and M. Kläui, Full angular dependence of the spin Hall and ordinary magnetoresistance in epitaxial antiferromagnetic NiO(001)/Pt thin films, *Phys. Rev. B* **98**, 024422 (2018).
- [11] S. Y. Bodnar, Y. Skourski, O. Gomonay, J. Sinova, M. Kläui, and M. Jourdan, Magnetoresistance Effects in the Metallic Antiferromagnet Mn<sub>2</sub>Au, *Phys. Rev. Appl.* **14**, 014004 (2020).
- [12] V. Grigorev, M. Filianina, S. Y. Bodnar, S. Sobolev, N. Bhattacharjee, S. Bommanaboyena, Y. Lytvynenko, Y. Skourski, D. Fuchs, M. Kläui, M. Jourdan, and J. Demsar, Optical Readout of the Néel Vector in the Metallic Antiferromagnet Mn<sub>2</sub>Au, *Phys. Rev. Appl.* **16**, 014037 (2021).
- [13] A. V. Kimel, B. A. Ivanov, R. V. Pisarev, P. A. Usachev, A. Kirilyuk, and T. Rasing, Inertia-driven spin switching in antiferromagnets, *Nat. Phys.* **5**, 727 (2009).
- [14] R. Cheng, M. W. Daniels, J.-G. Zhu, and D. Xiao, Ultrafast switching of antiferromagnets via spin-transfer torque, *Phys. Rev. B* **91**, 064423 (2015).
- [15] H. V. Gomonay and V. M. Loktev, Spin transfer and current-induced switching in antiferromagnets, *Phys. Rev. B* **81**, 144427 (2010).
- [16] J. Železný, H. Gao, K. Výborný, J. Zemen, J. Mašek, A. Manchon, J. Wunderlich, J. Sinova, and T. Jungwirth, Relativistic Néel-Order Fields Induced by Electrical Current in Antiferromagnets, *Phys. Rev. Lett.* **113**, 157201 (2014).
- [17] P. Wadley, *et al.*, Electrical switching of an antiferromagnet, *Science* **351**, 587 (2016).
- [18] A. Auerbach, *Interacting Electrons and Quantum Magnetism*, Graduate Texts in Contemporary Physics (Springer, New York, 1994).
- [19] T. Holstein and H. Primakoff, Field dependence of the intrinsic domain magnetization of a ferromagnet, *Phys. Rev.* **58**, 1098 (1940).
- [20] F. J. Dyson, General theory of spin-wave interactions, *Phys. Rev.* **102**, 1217 (1956).
- [21] S. V. Maleev, Scattering of slow neutrons in ferromagnets, *Sov. Phys. JETP* **6**, 766 (1958).
- [22] J. Schwinger, On angular momentum, US Atomic Energy Commission (1952).
- [23] D. P. Arovas and A. Auerbach, Functional integral theories of low-dimensional quantum Heisenberg models, *Phys. Rev. B* **38**, 316 (1988).
- [24] A. Auerbach and D. P. Arovas, Spin Dynamics in the Square-Lattice Antiferromagnet, *Phys. Rev. Lett.* **61**, 617 (1988).
- [25] L. O. Manuel and H. A. Ceccatto, Magnetic and quantum disordered phases in triangular-lattice Heisenberg antiferromagnets, *Phys. Rev. B* **60**, 9489 (1999).
- [26] C. Timm and P. J. Jensen, Schwinger boson theory of anisotropic ferromagnetic ultrathin films, *Phys. Rev. B* **62**, 5634 (2000).
- [27] H. Feldner, D. C. Cabra, and G. L. Rossini, Ferromagnetic frustrated spin systems on the square lattice: Schwinger boson study, *Phys. Rev. B* **84**, 214406 (2011).
- [28] T. N. De Silva, M. Ma, and F. C. Zhang, Pathology of Schwinger boson mean-field theory for Heisenberg spin models, *Phys. Rev. B* **66**, 104417 (2002).
- [29] M. Raykin and A. Auerbach,  $1/N$  expansion and spin correlations in constrained wave functions, *Phys. Rev. B* **47**, 5118 (1993).
- [30] M. Mathur, I. Raychowdhury, and R. Anishetty, SU( $N$ ) irreducible Schwinger bosons, *J. Math. Phys.* **51**, 093504 (2010).
- [31] E. A. Ghioldi, A. Mezio, L. O. Manuel, R. R. P. Singh, J. Oitmaa, and A. E. Trumper, Magnons and excitation continuum in  $XXZ$  triangular antiferromagnetic model: Application to Ba<sub>3</sub>CoSb<sub>2</sub>O<sub>9</sub>, *Phys. Rev. B* **91**, 134423 (2015).
- [32] M. R. Walther, D.-B. Hering, G. S. Uhrig, and K. P. Schmidt, Continuous similarity transformation for critical phenomena: Easy-axis antiferromagnetic  $XXZ$  model, *Phys. Rev. Res.* **5**, 013132 (2023).
- [33] S.-S. Zhang, E. A. Ghioldi, L. O. Manuel, A. E. Trumper, and C. D. Batista, Schwinger boson theory of ordered magnets, *Phys. Rev. B* **105**, 224404 (2022).
- [34] N. D. Mermin and H. Wagner, Absence of Ferromagnetism or Antiferromagnetism in One- or Two-Dimensional Isotropic Heisenberg Models, *Phys. Rev. Lett.* **17**, 1133 (1966).
- [35] L. Onsager, Crystal statistics. I. A two-dimensional model with an order-disorder transition, *Phys. Rev.* **65**, 117 (1944).
- [36] A. L. Chernyshev and M. E. Zhitomirsky, Spin waves in a triangular lattice antiferromagnet: Decays, spectrum renormalization, and singularities, *Phys. Rev. B* **79**, 144416 (2009).